Nonenzymatic Template-Directed RNA Synthesis Inside Model Protocells

Katarzyna Adamala and Jack W. Szostak

Science **342**, 1098 (2013);
DOI: 10.1126/science.1241888

Science (print ISSN 0036-8075; online ISSN 1095-9203) is published weekly, except the last week in December, by the American Association for the Advancement of Science, 1200 New York Avenue NW, Washington, DC 20005.

16. M. Umetani *et al.*, *Nat. Med.* **13**, 1185–1192 (2007).
17. Materials and methods are available as supplementary materials on *Science* Online.
18. C. E. Connor *et al.*, *Cancer Res.* **61**, 2917–2922 (2001).
19. C. T. Guy, R. D. Cardiff, W. J. Muller, *Mol. Cell. Biol.* **12**, 954–961 (1992).
20. E. Y. Lin *et al.*, *Am. J. Pathol.* **163**, 2113–2126 (2003).
21. M. Hansson, E. Ellis, M. C. Hunt, G. Schmitz, A. Babiker, *Biochim. Biophys. Acta* **1593**, 283–289 (2003).
22. A. Sica *et al.*, *Semin. Cancer Biol.* **18**, 349–355 (2008).
23. M. A. Lyons, A. J. Brown, *Lipids* **36**, 701–711 (2001).
24. G. Llaverias *et al.*, *Am. J. Pathol.* **178**, 402–412 (2011).
25. N. Alikhani *et al.*, *Oncogene* **32**, 961–967 (2013).
26. R. Karuna *et al.*, *Atherosclerosis* **214**, 448–455 (2011).
27. P. M. Sullivan *et al.*, *J. Biol. Chem.* **272**, 17972–17980 (1997).

Acknowledgments: This work was funded by the NIH [grants K99CA172357 (E.R.N.) and R37DK048807 (D.P.M.)] and the U.S. Department of Defense (DOD) [grants BC085585 (E.R.N.) and DOD BC094960 (D.P.M.)]. The content of this paper is solely the responsibility of the authors and does not necessarily represent the official views of the NIH or DOD.

Expression profiling data on 27HC in MCF7 cells were uploaded to Gene Expression Omnibus (GEO) (accession no. GSE46924) and were part of a larger study (GEO accession no. GSE35428).

Supplementary Materials

www.sciencemag.org/content/342/6162/1094/suppl/DC1
Materials and Methods
Supplementary Text
Figs. S1 to S14
References (*28*–*33*)

13 June 2013; accepted 25 October 2013
10.1126/science.1241908

Nonenzymatic Template-Directed RNA Synthesis Inside Model Protocells

Katarzyna Adamala[1,2] and Jack W. Szostak[1]*

Efforts to recreate a prebiotically plausible protocell, in which RNA replication occurs within a fatty acid vesicle, have been stalled by the destabilizing effect of Mg^{2+} on fatty acid membranes. Here we report that the presence of citrate protects fatty acid membranes from the disruptive effects of high Mg^{2+} ion concentrations while allowing RNA copying to proceed, while also protecting single-stranded RNA from Mg^{2+}-catalyzed degradation. This combination of properties has allowed us to demonstrate the chemical copying of RNA templates inside fatty acid vesicles, which in turn allows for an increase in copying efficiency by bathing the vesicles in a continuously refreshed solution of activated nucleotides.

The RNA world hypothesis suggests that the primordial catalysts were ribozymes (*1*, *2*), whereas biophysical considerations suggest that the primordial replicating compartments were membranous vesicles composed of fatty acids and related amphiphiles (*3*, *4*). However, the conditions required for RNA replication chemistry and fatty acid vesicle integrity have appeared to be fundamentally incompatible (*5*) (fig. S1). Both ribozyme-catalyzed and nonenzymatic RNA copying reactions require high (50 to 200 mM) concentrations of Mg^{2+} (or other divalent) ions (*6*), but Mg^{2+} at such concentrations destroys vesicles by causing fatty acid precipitation.

We developed a screen for small molecules that protect oleate fatty acid vesicles from disruption by Mg^{2+}. We used two assays to monitor the leakage of either a small charged molecule (calcein) or a larger oligonucleotide, allowing us to distinguish between increased membrane permeability (faster calcein release with oligonucleotide retention) and generalized membrane disruption (rapid release of both calcein and the oligonucleotide) (figs. S2 to S4). We identified several chelators, including citrate, isocitrate, oxalate, nitrilotriacetic acid (NTA), and EDTA, that protect oleate vesicles in the presence of at least 10 mM Mg^{2+} (figs. S5 and S6). In the presence of chelated Mg^{2+}, oleate vesicles remained intact but exhibited a modest increase in the permeability of a small polar molecule (Fig. 1 and fig. S7) and an even smaller increase in the leakage of an oligonucleotide. In terms of vesicle stabilization, citrate was one of the most effective chelators of Mg^{2+}.

We also examined the stability of model protocell membranes made of myristoleic acid:glycerol monomyristoleate (2:1) and from the more prebiotically reasonable decanoic acid:decanol:glycerol monodecanoate (4:1:1). Citrate-chelated Mg^{2+} caused only a small amount of leakage from these vesicles, and the stabilizing effect of citrate was seen for both calcein and oligonucleotides (Fig. 1 and figs. S8 to S13).

We then asked whether these chelators were compatible with the Mg^{2+} catalysis of nonenzymatic template-directed RNA primer extension. We measured the rate at which an RNA primer was elongated when annealed to an oligonucleotide with a templating region of C nucleotides, in the presence of an excess of the activated G monomer guanosine 5′-phosphor(2-methyl)imidazolide (2MeImpG) (Fig. 2). We examined citric acid, EDTA, NTA, and a weakly stabilizing chelator (isocitric acid). In the presence of 50 mM unchelated Mg^{2+}, the primer-extension reaction proceeded at a rate of 1.4 $hour^{-1}$, compared to 0.03 $hour^{-1}$ in the absence of Mg^{2+} ions. The addition of four equivalents of EDTA or NTA resulted in complete abolition of Mg^{2+} catalysis (Fig. 2 and figs. S14 and S15), indicating that the Mg^{2+} in these samples is chelated in a fashion incompatible with promoting primer extension. In contrast, four equivalents of citrate only decreased the rate of primer extension to 0.67 $hour^{-1}$. For comparison, isocitric acid does not fully protect vesicles (figs. S16 and S17) but also does not affect the primer extension reaction.

To see whether citrate would allow nonenzymatic RNA copying to proceed within fatty acid vesicles, we encapsulated an RNA primer-template complex inside oleate vesicles, added Mg^{2+} and citrate, and removed unencapsulated RNA by size exclusion chromatography. We then added the activated G monomer 2MeImpG, heated the sample briefly to allow for rapid monomer permeation (*7*), and then incubated it at room temperature for times up to 24 hours to allow

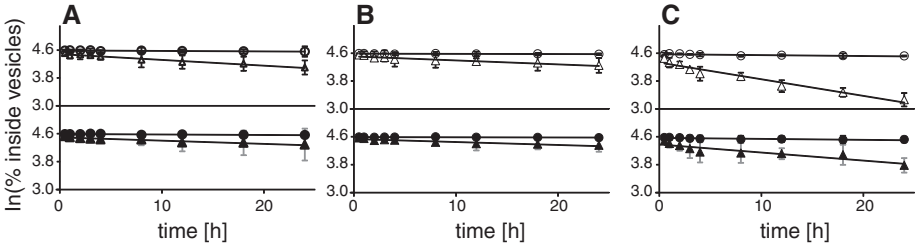

Fig. 1. Citrate stabilizes fatty acid vesicles in the presence of Mg^{2+} ions. Leakage of a small charged molecule (calcein, open symbols) and a larger nine-oligomer oligodeoxynucleotide (solid symbols) from fatty acid vesicles is shown. (**A**) Oleate vesicles; (**B**) myristoleate:glycerol monomyristoleate 2:1 vesicles; (**C**) decanoate:decanol:glycerol monodecanoate 4:1:1 vesicles. Circles, no $MgCl_2$, no citrate; triangles, 50 mM $MgCl_2$, 200 mM Na^+-citrate. The assay used to obtain these data is described in fig. S3. Lines are linear fits, coefficient of determination (R^2) ≥ 0.97. All experiments were repeated twice; error bars are mean ±2 SE.

[1]Howard Hughes Medical Institute, Department of Molecular Biology, and Center for Computational and Integrative Biology, Massachusetts General Hospital, Boston, MA 02114, USA. [2]Dipartimento di Biologia, Università degli Studi di Roma Tre, Rome, Italy.

*Corresponding author at Howard Hughes Medical Institute, Department of Molecular Biology, and Center for Computational and Integrative Biology, 7215 Simches Research Center, Massachusetts General Hospital, 185 Cambridge Street, Boston, MA 02114, USA. E-mail: szostak@molbio.mgh.harvard.edu

the monomer to take part in template-copying chemistry inside the vesicles. Analysis of the reaction products showed that after 24 hours of incubation, most of the primer had been extended by the addition of six G residues, with a smaller fraction extended to full length by the addition of a seventh G residue (Fig. 3). In parallel experiments with vesicles composed of mixtures of shorter-chain lipids, the brief heating step was not

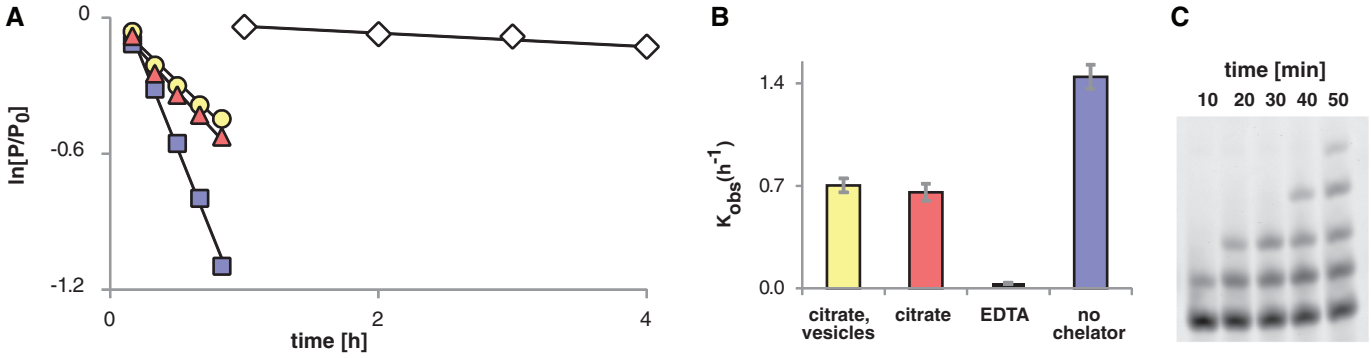

Fig. 2. The rate of RNA template-directed primer extension in the presence or absence of Mg^{2+} chelators and fatty acid vesicles. (**A**) Time courses of primer extension on a templating region of four C residues, expressed as a fraction of unextended primer remaining versus time. Squares, no chelators; triangles, 200 mM Na^+-citrate; circles, 200 mM Na^+-citrate and 100 mM oleate vesicles; diamonds, 200 mM EDTA. Lines are linear fits, $R^2 \geq 0.97$; the slope is k_{obs} ($hour^{-1}$). (**B**) Rates of primer extension under the indicated conditions; each kinetic experiment was performed in duplicate, and rates are determined as an average of the three separate runs. Error bars indicate SEM, $n = 3$ independent repetitions. (**C**) Typical polyacrylamide gel electrophoresis (PAGE) analysis of a template-directed primer extension experiment. Primer extension was carried out in the presence of 200 mM Na^+-citrate. For the gel analysis of the reactions used to obtain this data, see fig. S15.

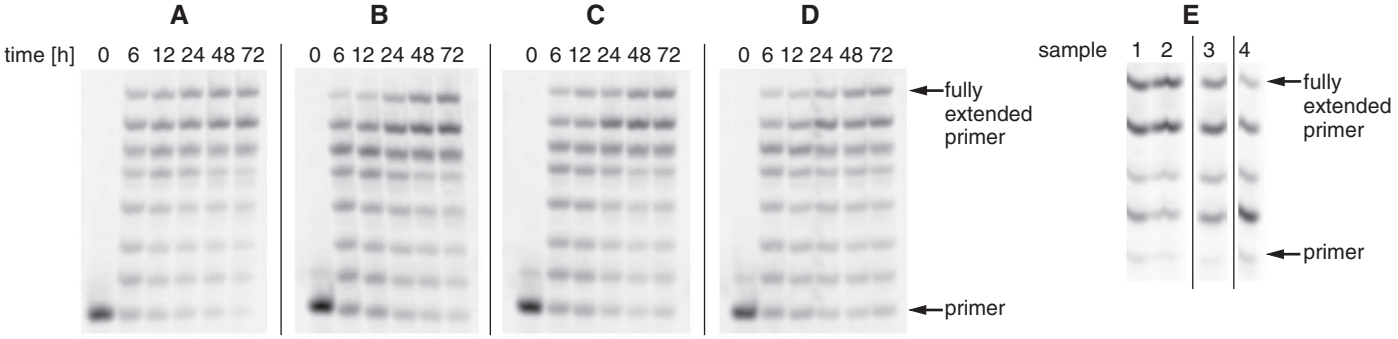

Fig. 3. RNA template copying inside model protocell vesicles. (**A** to **D**) Primer extension on a templating region of seven C residues. (A) Control reaction in solution; (B) inside oleate vesicles; (C) inside myristoleate:glycerol monomyristoleate 2:1 vesicles; (D) inside decanoate:decanol:glycerol monodecanoate 4:1:1 vesicles. (**E**) Extension of labeled RNA primer annealed to a mixed base template, templating region sequence GCCG. Sample 1, reaction inside myristoleate:glycerol monomyristoleate 2:1 vesicles; sample 2, reaction inside decanoate:decanol:glycerol monodecanoate 4:1:1 vesicles. Both sample 1 and 2 reactions were performed inside a liposome dialyzer (see the supplementary materials for the description of the liposome dialyzer) with a total of 13 buffer exchanges. Sample 3, control reaction in solution with daily addition of fresh portion of activated monomers, without removing the hydrolyzed monomers. Sample 4, control reaction in solution, without the addition of fresh monomer.

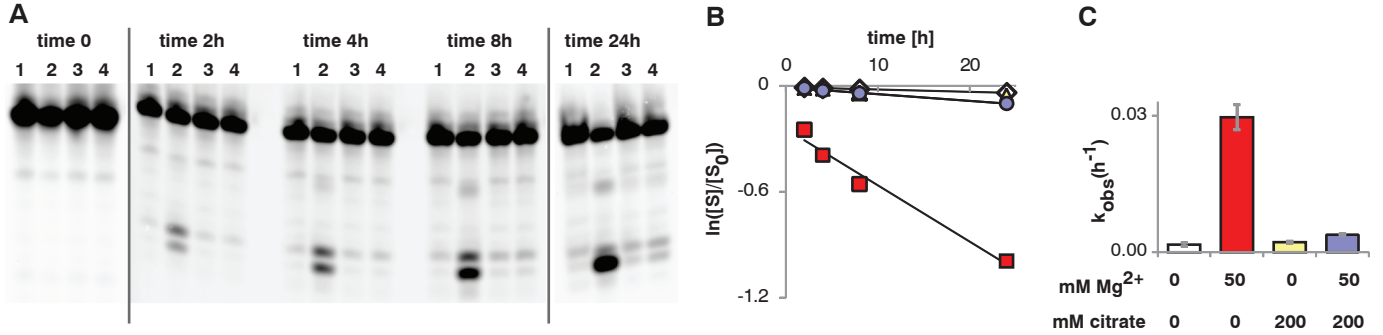

Fig. 4. Citrate protects RNA from Mg^{2+}-catalyzed degradation. (**A**) PAGE analysis of cleavage of a DNA oligonucleotide at the site of a single internal ribonucleotide, at indicated time points; lane 1, no Mg^{2+}, no citrate; lane 2, 50 mM Mg^{2+}, no citrate; lane 3, no Mg^{2+}, 200 mM citrate; lane 4, 50 mM Mg^{2+}, 200 mM citrate. (**B**) Quantitation of strand cleavage, expressed as a fraction of the intact substrate over total substrate versus time. Diamonds, no Mg^{2+}, no citrate; triangles, no Mg^{2+}, 200 mM citrate; circles, 50 mM Mg^{2+}, 200 mM citrate; squares, 50 mM Mg^{2+}, no citrate. Lines are linear fits, $R^2 \geq 0.97$. (**C**) Rates of strand cleavage at the *ribo* linkage with and without Mg^{2+} and citrate. Error bars indicate SEM, $n = 3$ independent repetitions.

necessary, because of the higher permeability of such membranes to nucleotide monomers. It is noteworthy that RNA primer extension occurred efficiently inside vesicles made of decanoic acid: decanol:glycerol monodecanoate (4:1:1) (Fig. 3), because short-chain saturated amphiphilic compounds are more prebiotically plausible than longer-chain unsaturated fatty acids such as oleate or myristoleate. When we encapsulated the RNA primer-template complex inside POPC vesicles, no primer extension was observed, because of the impermeability of phospholipid vesicles to the 2MeImpG monomer (even with a heat pulse) (fig. S18).

The efficiency of nonenzymatic RNA replication can be greatly enhanced by the periodic addition of fresh portions of activated monomer to a primer-extension reaction occurring on templates immobilized by covalent linkage to beads (*8*). We sought to reproduce this effect by mimicking the flow of an external solution of fresh monomers over vesicles, by periodic dialysis of model protocells against a solution of fresh activated monomers (see the supplementary materials for a description of the liposome reactor dialyzer). The control primer-extension reaction in solution shows that the yield of full-length primer-extension product from copying a GCCG template is very low, even if fresh monomers are added to the reaction periodically (Fig. 3E). In contrast, after repeated exchanges of external solution by dialysis, the proportion of full-length product was much greater (Fig. 3E).

The high thermal stability of the RNA duplex is a major problem for prebiotic RNA replication (*5*). Because Mg^{2+} greatly increases the melting temperature (T_m) of RNA duplexes, we asked whether the chelating properties of citrate would prevent the increase in the T_m of RNA duplexes caused by the presence of free Mg^{2+} ions. We observed a small but reproducible decrease in T_m in the presence of citrate when compared to samples containing unchelated Mg^{2+} (table S1 and figs. S19 and S20). For example, in the presence of 50 mM Mg^{2+} with four equivalents of citrate, the T_m of the RNA duplex was 71°C, whereas in the control sample without citrate the T_m was 75°C.

Citrate also stabilizes RNA by preventing the Mg^{2+} catalysis of RNA degradation. Incubating a 13-oligomer oligodeoxynucleotide with one *ribo* linkage at 75°C, with and without Mg^{2+} and citrate, results in significant strand cleavage at the site of the single *ribo* linkage. Four equivalents of citrate, relative to Mg^{2+}, abolished the Mg^{2+}-catalyzed degradation (Fig. 4). The observed rate constant (k_{obs}) for cleavage at the *ribo* linkage, at 75°C in the presence of 50 mM Mg^{2+} was 0.03 $hour^{-1}$, whereas in the presence of a fourfold excess of citrate, the rate decreased to 0.004 $hour^{-1}$.

The chelation of Mg^{2+} by citrate exhibits two protective effects in the context of model protocells: Protocell membranes based on fatty acids are protected from the disruption caused by the precipitation of fatty acids as Mg^{2+} salts, and single-stranded RNA oligonucleotides are protected from Mg^{2+}-catalyzed degradation. Based on the known affinity of citrate for Mg^{2+} (*9*, *10*), it is clear that the RNA synthesis observed in the presence of Mg^{2+} and citrate cannot be due to residual free Mg^{2+} (less than 1 mM) and must be due to catalysis by the Mg^{2+}-citrate complex. The crystal structure of Mg^{2+}-citrate (*11*) shows that the Mg^{2+} ion is coordinated by the hydroxyl and two carboxylates of citrate, so that three of the six coordination sites of octahedral Mg^{2+} are occupied by citrate, while the remaining three are free to coordinate with water or other ligands. The clear implication is that coordination of Mg^{2+} by at most three sites is sufficient for catalysis of template-directed RNA synthesis, but not for catalysis of RNA degradation or for the precipitation of fatty acids. In the absence of a prebiotic citrate synthesis pathway [but see (*12*) for a recent advance], it is of interest to consider prebiotically plausible alternatives to citrate that could potentially confer similar effects, such as short acidic peptides. Just such a peptide constitutes the heart of cellular RNA polymerases, where it binds and presents the catalytic Mg^{2+} ion in the active site of the enzyme.

References and Notes

1. W. Gilbert, *Nature* **319**, 618 (1986).
2. G. F. Joyce, *Nature* **338**, 217–224 (1989).
3. J. M. Gebicki, M. Hicks, *Nature* **243**, 232–234 (1973).
4. D. W. Deamer, J. P. Dworkin, *Top. Curr. Chem.* **259**, 1–27 (2005).
5. J. W. Szostak, The eightfold path to non-enzymatic RNA replication. *J. Sys. Chem.* **3:2** (2012).
6. J. C. Bowman, T. K. Lenz, N. V. Hud, L. D. Williams, *Curr. Opin. Struct. Biol.* **22**, 262–272 (2012).
7. S. S. Mansy, J. W. Szostak, *Proc. Natl. Acad. Sci. U.S.A.* **105**, 13351–13355 (2008).
8. C. Deck, M. Jauker, C. Richert, *Nat. Chem.* **3**, 603–608 (2011).
9. A. K. Covington, E. Y. Danish, *J. Solution Chem.* **38**, 1449–1462 (2009).
10. M. Walser, *J. Phys. Chem.* **65**, 159–161 (1961).
11. C. K. Johnson, *Acta Crystallogr.* **18**, 1004–1018 (1965).
12. C. Butch *et al.*, *J. Am. Chem. Soc.* **135**, 13440–13445 (2013).

Acknowledgments: We thank A. Engelhart, C. Hentrich, A. Larsen, N. Kamat, and A. Björkbom for discussions and help with manuscript preparation and A. Gifford for help with vesicle leakage experiments. This work was supported in part by NASA Exobiology grant NNX07AJ09G. J.W.S. is an investigator of the Howard Hughes Medical Institute. Raw data are presented in the supplementary materials. The instructions for assembling the Liposome Dialyzer are available at http://molbio.mgh.harvard.edu/szostakweb/.

Supplementary Materials

www.sciencemag.org/content/342/6162/1098/suppl/DC1
Materials and Methods
Supplementary Text
Figs. S1 to S21
Tables S1 to S3
Liposome Dialyzer Instructions
References (*13*–*15*)

13 June 2013; accepted 25 September 2013
10.1126/science.1241888

Primate Transcript and Protein Expression Levels Evolve Under Compensatory Selection Pressures

Zia Khan,[1]* Michael J. Ford,[2] Darren A. Cusanovich,[1] Amy Mitrano,[1] Jonathan K. Pritchard,[1,3]*† Yoav Gilad[1]*

Changes in gene regulation have likely played an important role in the evolution of primates. Differences in messenger RNA (mRNA) expression levels across primates have often been documented; however, it is not yet known to what extent measurements of divergence in mRNA levels reflect divergence in protein expression levels, which are probably more important in determining phenotypic differences. We used high-resolution, quantitative mass spectrometry to collect protein expression measurements from human, chimpanzee, and rhesus macaque lymphoblastoid cell lines and compared them to transcript expression data from the same samples. We found dozens of genes with significant expression differences between species at the mRNA level yet little or no difference in protein expression. Overall, our data suggest that protein expression levels evolve under stronger evolutionary constraint than mRNA levels.

Measurements of mRNA levels have revealed substantial differences across primate transcriptomes (*1*–*3*) and have led to the identification of putatively adaptive changes in transcript expression (*4*). Traditionally, measurements of divergence in mRNA levels are assumed to be good proxies for divergence in protein levels. However, there are numerous mechanisms by which protein expression may be regulated independently of mRNA levels (*5*, *6*). If transcript and protein expression levels are often uncoupled, mRNA levels may evolve under reduced constraint as changes at the transcript level could be buffered or compensated for at the

[1]Department of Human Genetics, University of Chicago, Chicago, IL 60637, USA. [2]MS Bioworks, LLC, 3950 Varsity Drive, Ann Arbor, MI 48108, USA. [3]Howard Hughes Medical Institute, University of Chicago, Chicago, IL 60637, USA.

*Corresponding author. E-mail: zia@uchicago.edu (Z.K.); pritch@stanford.edu (J.K.P); gilad@uchicago.edu (Y.G.)
†Present address: Departments of Genetics and Biology, Stanford University, Stanford, CA 94305, USA.

www.sciencemag.org/content/342/6162/1098/suppl/DC1

Supplementary Material for

Nonenzymatic Template-Directed RNA Synthesis Inside Model Protocells

Katarzyna Adamala and Jack W. Szostak*

*Corresponding author. E-mail: szostak@molbio.mgh.harvard.edu

Published 29 November 2013, *Science* **342**, 1098 (2013)
DOI: 10.1126/science.1241888

This PDF file includes:

Materials and Methods

SupplementaryText

Figs. S1 to S21

Tables S1 to S3

Liposome dialyzer instructions

Full Reference List

Materials and Methods

Guanosine 5′-monophosphate was purchased as the free acid from MP Biomedicals. RNAse free water, Tris-Cl buffer stock, $MgCl_2$, EDTA and NaCl were purchased from Ambion. All other chemicals were purchased from Sigma Aldrich and were used without further purification. All oligonucleotides were purchased from IDT DNA and HPLC purified by the manufacturer. Fluorescently labeled oligonucleotide products of primer extension reaction were separated by PAGE and imaged with an Amersham Biosciences Typhoon 9410.

Formation of fatty acid vesicles

A thin film of lipids was prepared by evaporating a chloroform solution of lipids. Vesicles were formed by rehydration of the film with buffer, usually 0.25 M Tris-Cl pH 8 with an additional 0.5 equivalents of NaOH (relative to non-esterified carboxylic acid residues present in the lipid preparation). Samples were vortexed for about a minute and then tumbled at room temperature for 16 to 18 hours. Small unilamellar vesicles were prepared by 7 passages through a 100 nm pore membrane (Avanti Polar Lipids) using a Mini-Extruder (Avanti Polar Lipids). Vesicles were tumbled for at least 1 h after extrusion.

During the course of our experiments, we discovered that making vesicles with K+ instead of Na^+ makes vesicles much less prone to aggregation after mixing with chelated Mg^{2+} ions. If NaOH is used (to form vesicles and to adjust pH of the acid chelator) vesicles need to be tumbled very rapidly at all times to prevent aggregation. Substituting KOH makes it possible to tumble the vesicles more slowly, at a rate comparable to that required to prevent aggregation of vesicles prepared in the absence of Mg^{2+} ions.

Permeability of vesicles to oligonucleotides (kinetic assay)

Vesicles containing encapsulated DNA were prepared as described above except that the rehydration solution contained 200 μM Cy3-labeled acceptor oligodeoxynucleotide. Vesicles prepared with acceptor oligodeoxynucleotide were purified on a Sepharose 4B size exclusion column to remove unencapsulated oligodeoxynucleotide. The vesicle fraction was collected and tumbled for ~1 h. Purified vesicles were mixed with empty vesicles (to increase the lipid concentration to 75 mM total lipid in the final sample) and with donor (FAM-labeled) oligodeoxynucleotide, and then a pre-mixed solution of $MgCl_2$ and the chelator to be tested was added. Samples were briefly vortexed and immediately placed in the wells of 384 well plate. Chelator and magnesium were always pre-mixed at given ratio and equilibrated for at least 1h before adding to vesicle sample, to avoid exposure of vesicles to unchelated Mg^{2+} ions. Leakage of the oligodeoxynucleotide from purified vesicles was followed by monitoring FRET between the FRET acceptor 5′-Cy3-d(GCG CAT TGG)-3′ encapsulated inside vesicles and the FRET donor 5′-d(CCA ATG CGC)-3′-FAM added to the outside of the vesicles.

The final concentration of donor DNA oligo was typically 0.5 μM; for each purified vesicle sample the donor oligonucleotide concentration was adjusted so that the measured Fdonor/Facceptor ratio was 2 to 3 for the vesicle sample and decreased to ~0.2 after lysis of vesicles with 10% Triton X-100. The donor concentration was adjusted to compensate for differences in the efficiency of encapsulation and purification of acceptor

vesicles between different vesicle preparations. Fluorescence was recorded over 42 to 45 h at an excitation wavelength of 485 nm and emission wavelengths of 520 nm and 564 nm. The reported FRET signal is the ratio $F_{donor}/F_{acceptor}$ between the acceptor dye Cy3 and the donor dye FAM. As acceptor oligodeoxynucleotide leaks from vesicles and hybridizes with external donor oligodeoxynucleotide, fluorescence of the donor FAM (Fdonor) decreases and fluorescence of the acceptor Cy3 ($F_{acceptor}$) increases.

Permeability of vesicles to calcein (kinetic assay)

All vesicles were prepared with 20 mM calcein, purified and mixed witch tested chelators as described above.

The reported ratio of fluorescence of the vesicle sample to total fluorescence (F_{ves}/F_{total}) is the ratio of fluorescence measured at a given time, typically 42 to 45 h, to the fluorescence of the completely dequenched calcein in the sample measured after lysing vesicles with 10% Triton X-100. Vesicles start with 20 mM encapsulated calcein, and as a result of self-quenching the initial fluorescence intensity is low; as the calcein leaks out of the vesicles, it is diluted in the external buffer and the fluorescence intensity increases.

Leakage of calcein and oligonucleotides from vesicles (column purification assay)

Vesicles were prepared with 5 mM calcein or 200 μM of the DNA oligonucleotide 5′-Cy5 GCG CAU UGG-3′ and purified as described above. After tumbling for 4 h at RT, samples of vesicles with chelator and Mg^{2+} were purified by size exclusion chromatography. During the purification, the mobile phase was buffer with 75 mM lipid and the given $MgCl_2$ and chelator concentration, so the total concentration of lipid and the ratio of lipid to Mg^{2+} and chelator stayed constant during the purification. Vesicle fractions were collected, pooled and tumbled at RT. At the indicated time points, an aliquot of vesicles was removed and re-purified by size-exclusion chromatography, with 75 mM lipid and the given Mg^{2+} and chelator concentrations in the mobile phase. Fluorescence in the vesicle and free fractions was measured. The reported fraction encapsulated vs. time represents the fraction of the fluorescence remaining in the vesicle fraction after the second column purification.

Synthesis of activated RNA monomers

Guanosine 5′-phosphor-2-methylimidazolide (2MeImpG) and cytosine 5′-phosphor-2-methylimidazolide (2MeImpC) were synthesized according to the literature procedure (13). The 2MeImpG was obtained as a white powder in 81% yield and the 2MeImpC was obtained as a white powder in 88% yield.

RNA primer and template oligonucleotides

RNA template copying reactions were performed using two different sets of primers and templates. Both primer / template pairs form stable duplexes at 25° C (Table S2).

For the primer extension of 4 G residues: primer-G1: 5′-Cy3-GCGUAGACUGACUG-3′; template-C4: 5′-ACCCCCAGUCAGUCUACGC-3′. For the primer extension of 7 G residues: primer-G2: 5′-Cy3-GCGUAGACUGACUGG-3′; template-C7: 5′-AACCCCCCCCCAGUCAGUCUACGC-3′. For the mixed base

extension: primer-GC 5′-Cy3-GCGUAGACUGACUGG -3′, template-GC 5′-AGCCGCCAGUCAGUCUACGC-3′.

Kinetics of RNA template copying in the presence of citrate

RNA template copying reactions contained a final concentration of 2 μM primer-G1, 10 μM template-C4, 50 mM 2MeImpG, 50 mM $MgCl_2$ and 0.25 M Tris-Cl buffer pH 8.0. A stock solution of citric acid, used to prepare samples with citrate, was adjusted to the reaction pH with NaOH. Samples were incubated at 20° C in a thermal cycler, and 30 μL aliquots were collected at the indicated time points and immediately precipitated with EtOH. Samples were kept at -20° C for 30 minutes, then centrifuged, and the RNA pellet washed with 70% EtOH and dissolved in 8 M Urea 1x TBE loading buffer. Samples were analyzed by TBE-Urea 20% PAGE. Gels were scanned on an Amersham Typhoon imager and quantified using GelQuant.NET version 1.8.1 by Biochem Lab Solutions. The kinetic experiments were done using the same batch of 2MeImpG for all directly compared experiments. The pseudo-first order reaction rate was determined from the slope of linear fits of the natural logarithm of the ratio of the amount of unreacted primer remaining at a given time point to the total of all primer plus extended primer species, plotted vs. time.

RNA template copying in protocell vesicles

Vesicle samples were prepared with 0.1 M of total lipid, 50 μM primer and 150 μM template in 0.25 M Tris-Cl pH 8.0. Samples were tumbled for 12 h, extruded and equilibrated for 1 h. Samples were then mixed with a stock solution of $MgCl_2$ and Na^+-citrate to give a final total lipid concentration of 75 mM. Vesicles were purified on a Sepharose 4B size exclusion column, with 0.25 M Tris-Cl pH 8.0, 75 mM lipid, and the indicated concentrations of $MgCl_2$ and Na^+-citrate as the mobile phase. Vesicle fractions were collected and pooled. Template copying reactions were started by adding 2MeImpG to a final concentration of 50 mM, after which samples were vortexed and vigorously tumbled at room temperature. After incubation for the indicated times, an aliquot of vesicles was purified a second time by size exclusion chromatography, this time with only Tris-Cl pH 8.0 as mobile phase (except decanoic acid : decanol : glycerol monodecanoate vesicles which was was purified with 5 mM lipids in the mobile phase). Vesicle and small molecule fractions were collected. The vesicle fraction was mixed with Triton X-100 to 1% v/v and then precipitated with cold ethanol at -20°C for 1 h, then centrifuged; the RNA pellets were washed with 70% cold ethanol, dissolved in 8M Urea 1x TBE loading buffer and samples were analyzed by TBE-Urea 20% PAGE.

The fully extended primer contained a long poly-G region, resulting in poor resolution of the elongated primer species by PAGE. To increase gel resolution and prevent smearing of the bands gel analysis of template-C7 copying reactions was performed with Li^+-TBE buffer instead of the standard Na^+-TBE buffer.

Mixed template RNA template copying in protocell vesicles with dialysis

Vesicle samples were prepared as described above. Vesicles with RNA were transferred to the reaction chamber of the liposome dialyzer reactor. The buffer exchange chamber was filled with solution containing an equal concentration of fatty acid vesicles, magnesium, citrate, and activated monomers as the initial sample. Each buffer exchange

was done with the same volume and same concentration of fatty acid vesicles, magnesium, citrate, and activated monomers as the initial sample. Typically dialysis buffer was exchanged every 12 hours through the course of the reaction.

Melting temperatures of RNA duplexes in the presence of citrate

All samples were prepared by mixing stock solutions of RNA oligonucleotides 5′-CAGUCAUGUAGUC and 5′-GACUACAUGACUG to a final concentration of 15 μM of each RNA strand, with 1 mM EDTA, 0.1 M NaCl and 0.25 M Tris-Cl pH 8.0 in each sample. Thermal denaturation of RNA was monitored using 1 mm quartz cuvettes (Starna) in an Agilent Cary 60 UV spectrophotometer interfaced to a Quantum Northwest LC 600 6-position Peltier temperature controller with the Agilent ADL controller and LC 600 serial interface, using a melting cycle program written by Dr. Aaron Engelhart. At each temperature step the system was allowed to equilibrate at the setpoint until it was within 0.25 ^{o}C of the setpoint for 30 seconds, at which point a spectrum was collected. This resulted in a temperature increase of about 0.45 ^{o}C min^{-1}. Melting temperatures were determined by a sigmoid fit of the recorded A260, using the first forward (heating) trace. Each sample was prepared in duplicate; the reported Tm is the arithmetic average of the two measurements.

Determination of the rate of Mg^{2+} catalyzed RNA degradation with and without citrate

20 μL samples containing 5 μM of the oligonucleotide 5′-Cy5-CAGUCAUrGUAGUC and 1 mM EDTA in 0.25 M Tris-Cl pH 8.0 were incubated at 75 °C in a thermal cycler for the indicated times, with and without 50 mM $MgCl_2$ and with and without 200 mM Na^{+}-citrate. At each time point, samples were removed from the thermal cycler, purified using ZipTip C18 Pipette Tips (Milipore), then analyzed by TBE-Urea 20% PAGE. The amounts of remaining full length oligonucleotide and of hydrolysis products were quantified, and fitted to a pseudo-first order reaction equation to obtain k_{obs} values for strand cleavage at the single ribo site.

Supplementary Text

Membrane fluidity in presence of Mg^{2+} and citrate

In order to better understand the changes to the structure of the bilayer fatty acid membrane in the presence of chelated Mg^{2+}, we have measured the fluorescence polarization anisotropy of 1,6-diphenyl-l,3,5-hexatriene (DPH) in oleate membranes in the presence of Mg^{2+} and citrate. Changes in anisotropy correspond to changes in the fluidity of the membrane. At 4 equivalents of citrate to magnesium, we observed that the membrane anisotropy decreases with increasing Mg^{2+} concentration. This suggests that in presence of Mg^{2+}-citrate, the oleate bilayer membrane becomes less rigid, which is consistent with the observed increase in permeability (Figure S21).

To determine the anisotropy of DPH in fatty acid vesicle membranes, oleate vesicles were prepared as described above, with 1,6-diphenyl-l,3,5-hexatriene (DPH) at a ratio of 1:400 DPH:oleate. After extrusion, samples were mixed with different stock solutions of $MgCl_2$ and Na^+-citrate, so as to give a 75 mM oleate solution, the desired concentration of $MgCl_2$, and 4 equivalents of citrate to magnesium. Samples were vigorously tumbled for 1 hour, and then diluted to 4 mM oleate for measurements. The steady state fluorescence anisotropy was measured at an excitation wavelength of 360 nm and an emission wavelength of 430 nm, with g factor = 1, using a Cary Eclipse fluorimeter (Varian, Mulgrave, Australia) with Manual Polarizer Accessory by Varian. Fluorescence anisotropy was calculated as a unitless ratio defined as $R = (I_{=} - I_{\perp})/(I_{=} + 2I_{\perp})$, where I is the emission intensity parallel ($I_{=}$) or perpendicular ($I_{\perp}$) to the direction of polarization of the excitation source.

Thermal stability of duplex RNA in the presence of Mg^{2+}, citrate and fatty acid vesicles

We measured the T_m of a 10-mer RNA duplex in the presence of oleate vesicles. Because of the high turbidity of the solution, it was impossible to use the standard method of monitoring the absorbance of the sample. Instead we used the FRET (Fluorescence Resonance Energy Transfer) effect instead. The RNA oligonucleotides used in this experiment were 5′-r(GACUACAUGACUG Cy5) and 5′-r(Cy3 CAGUCAUGUAGUC). In the hybridized duplex, the efficiency of FRET between the dyes is high, and it decreases as the strands melt apart. We have measured the T_m of this RNA duplex with and without fatty acid vesicles, and with and without 50 mM Mg^{2+} with 4 equivalents of Na^+-citrate. We observed that without Mg^{2+}, the presence of 75 mM oleic acid vesicles did not affect the T_m of the duplex. In samples with vesicles the Tm was 63 °C and without vesicles the T_m was 63 °C, compared to 64°C in control sample with NaCl (to equal salt concentration), which is within the experimental error. In samples with Mg^{2+} and Na^+-citrate, the T_m of the RNA in the absence of vesicles was 68 °C, and in the presence of 75 mM oleate vesicles was 69 °C (Tables S1 and S3).

Therefore, we conclude that the presence of fatty acid membranes does not affect the stability of the RNA duplex.

It was impossible to measure the T_m of RNA in the presence of vesicles with unchelated Mg^{2+} because the oleate immediately precipitates.

Oleate vesicles were prepared as described above. 30 uL samples were prepared by mixing vesicles with stock solutions of RNA, Na^+-citrate and $MgCl_2$, to a final concentration of 100 mM oleic acid, 5 μM of each of the RNA oligonucleotides, and 50 mM $MgCl_2$ with 200 mM Na^+-citrate where indicated. Vesicle samples were always mixed with pre-mixed $MgCl_2$ and Na^+-citrate stock, to avoid exposing vesicles to unchelated Mg^{2+} ions. After mixing, vesicles were vortexed for about 5 min and vigorously tumbled for 1.5 hour. All samples were prepared in triplicate. Samples were placed on an RT-PCR FAST 96 well plate and the RNA melting curve, as reported by Cy3 fluorescence vs. temperature, was recorded using an Applied Biosystems 7500/7500 Fast Real-Time PCR machine.

Separate samples were prepared with only the Cy3 labeled oligonucleotide. Each Cy3 melting curve of RNA was normalized to the fluorescence of the Cy3 dye in the sample without the acceptor dye Cy5 by dividing the Cy3 signal in sample with acceptor by the Cy3 signal without acceptor, to compensate for temperature changes in the fluorescence of the dye independent of the FRET effect between the Cy3 and Cy5 dyes. Melting temperatures were determined by a sigmoid fit of the recorded Cy3 normalized fluorescence, using the first forward trace.

Figure S1.

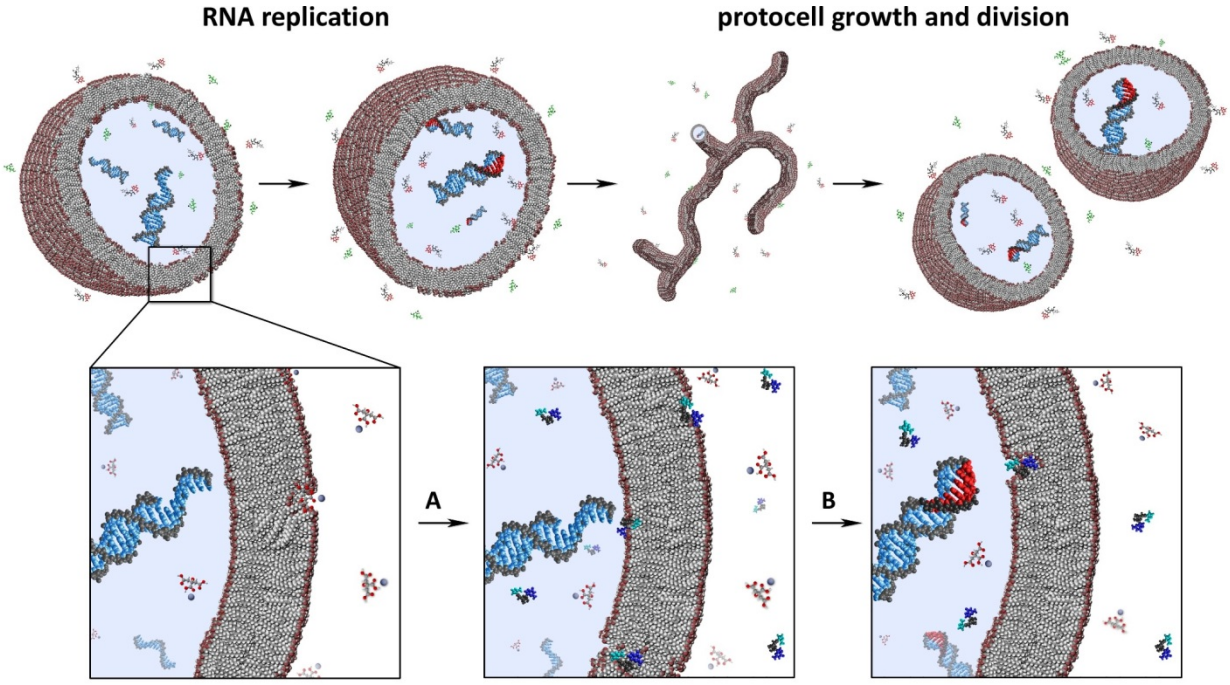

Figure S1. General scheme for non-enzymatic template-directed RNA synthesis inside vesicles.
Top: RNA is encapsulated inside protocell vesicles; the addition of activated monomers, in the presence of Mg^{2+} ions, leads to the copying of the RNA template. Protocells grow by absorbing additional fatty acid molecules from added fatty acid micelles, develop into filamentous vesicles and subsequently divide in response to shear stresses (*14, 15*).
Bottom: Protocell vesicles contain encapsulated primer-template RNA, and are stable in the presence of Mg^{2+} ions chelated by citrate; A, activated monomers cross the fatty acid bilayer membrane, and B, take part in template copying RNA synthesis.

Figure S2.

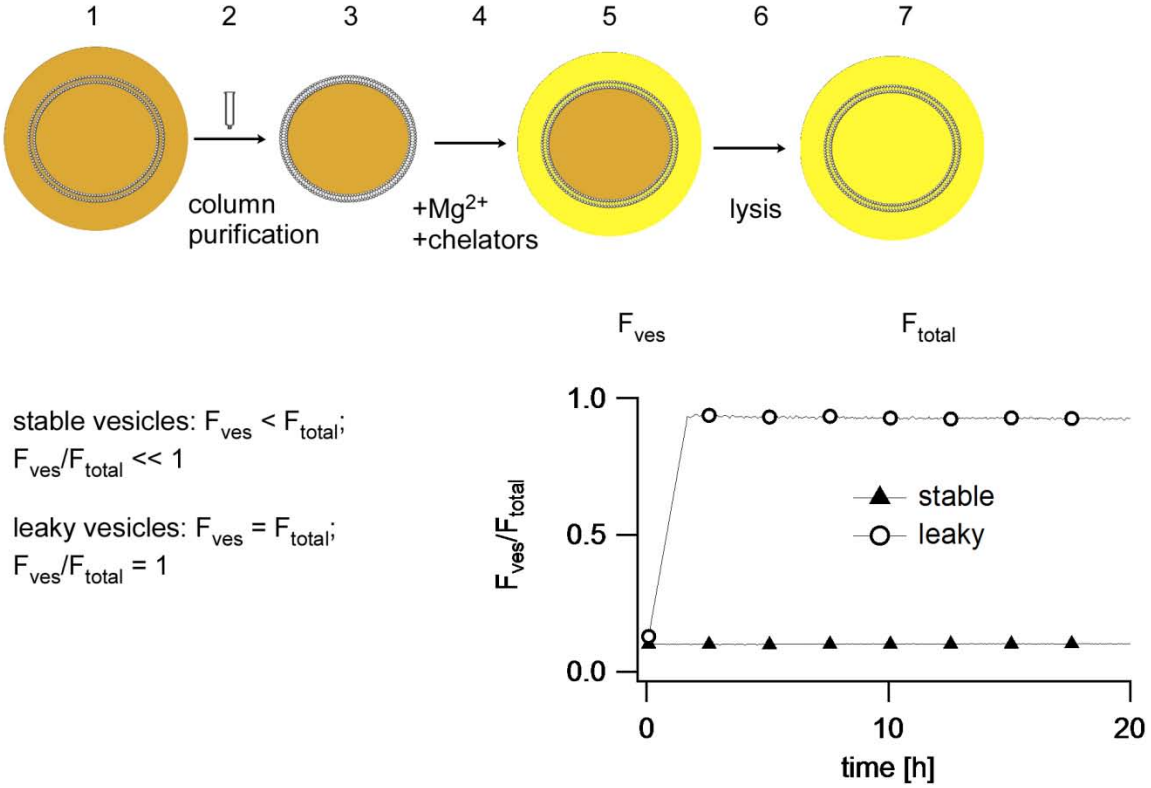

Figure S2. Schematic representation of the assay used to estimate leakage of calcein from vesicles over time.

1: Vesicles were prepared as described in Materials and Methods, with 20 mM calcein.
2: Vesicles were purified on a Sepharose 4B size exclusion column to remove unencapsulated calcein. The fraction containing vesicles was collected.
3: Vesicles with encapsulated acceptor oligo were mixed with empty oleate vesicles (to bring the total lipid concentration to 75 mM). At this point, all calcein was encapsulated inside vesicles, self-quenched at 20 mM.
4. Samples were mixed with pre-mixed $MgCl_2$ and chelator at a given ratio, so that vesicles were never exposed to unchelated Mg^{2+}.
5. Samples were placed on 386 multi-well plate and fluorescence was recorded over a given time (usually 40 hours) at λ_{ex} 485nm, λ_{em} 520nm. If vesicles were permeable, calcein would leak out and the fluorescence would increase, as a result of dequenching of the calcein as it is diluted in the external buffer.
6. Vesicles were lysed with 1% (w/w) Triton X-100.
7. Fluorescence was again recorded, giving the total fluorescence of unquenched calcein in the sample. The permeability of the vesicles was estimated from the rate at which the fluorescence of encapsulated calcein increased over time. The plot shows the ratio of fluorescence measured during the time course of the experiment (before lysis, F_{ves}) to the total fluorescence of the dequenched calcein (F_{total}).

Figure S3.

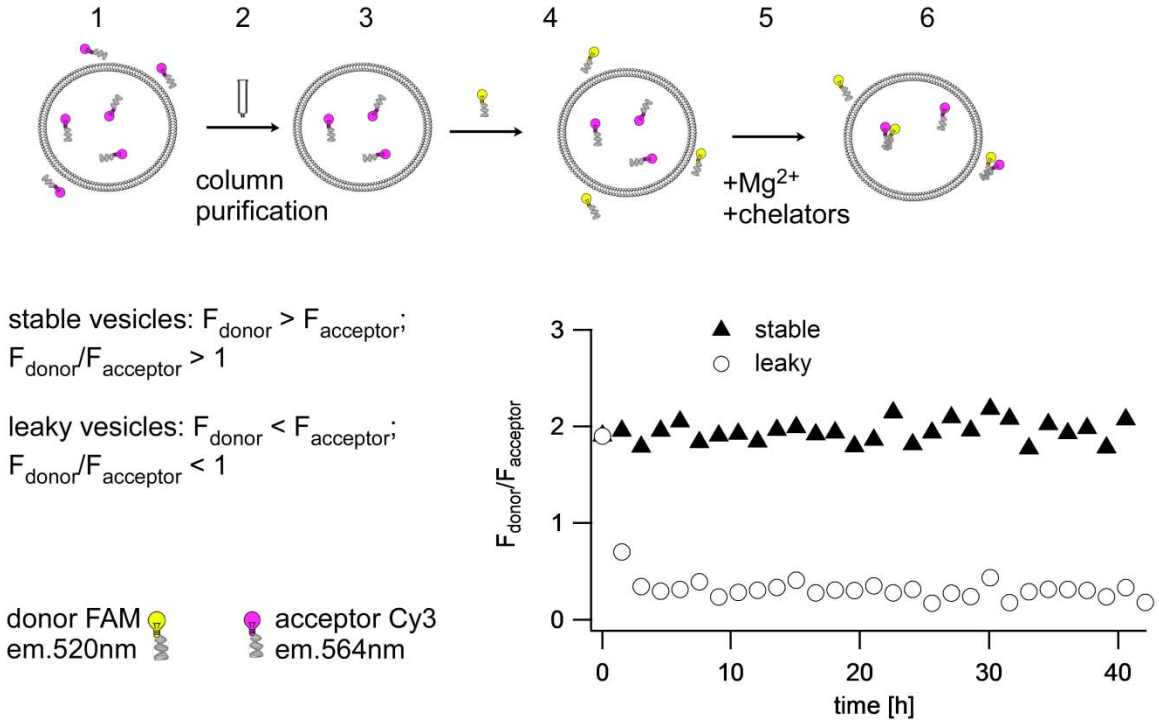

Figure S3. Schematic representation of assay used to estimate leakage of oligonucleotides from vesicles over time.
1: Vesicles were prepared as described in Materials and Methods, with 200 µM acceptor oligonucleotide d(Cy3-5′-GCGCATTGG-3′).
2: Vesicles were purified on Sepharose 4B size exclusion column to remove unencapsulated oligonucleotide.
3. The fraction containing vesicles was collected. Vesicles with encapsulated acceptor oligo were mixed with empty oleate vesicles, to bring the total lipid concentration to 75 mM.
4: Donor oligo d(5′-CCAATGCGC -3′-FAM) was added to the vesicle sample. At this point, acceptor oligo was encapsulated inside vesicles and donor oligo is outside vesicles.
5. Samples were mixed with a previously prepared stock of $MgCl_2$ and chelator at a given ratio; vesicles were always mixed with premixed magnesium and chelator, so that vesicles were never exposed to unchelated magnesium.
6. Samples were placed in a 386 multi-well plate and fluorescence was recorded for a given time (usually 40 hours) at λ_{ex} 485nm, λ_{em} 520nm and 564nm. FRET signal is calculated as ratio of F_{donor} to $F_{acceptor}$.

Figure S4.

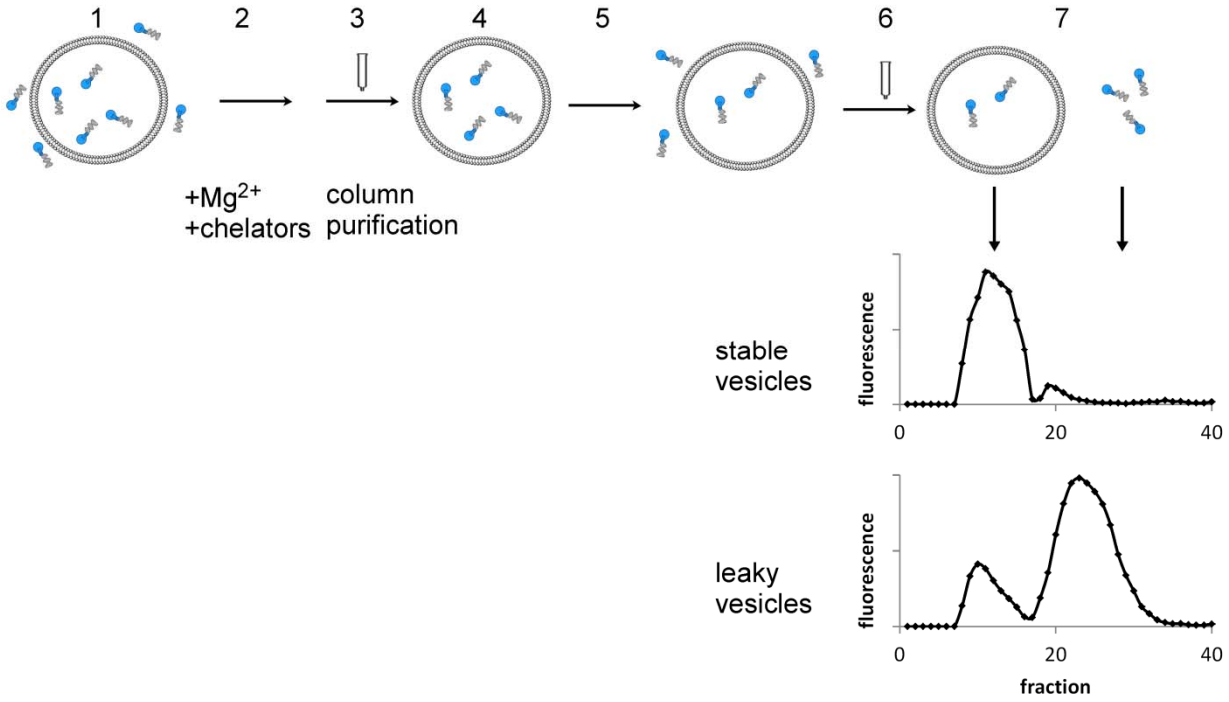

Figure S4. Schematic representation of vesicle purification assay used to calculate leakage of oligonucleotides from vesicles at given time points.
1: Vesicles were prepared as described in Materials and methods, with 200 μM oligonucleotide d(Cy5-5′-GCG CAT TGG-3′).
2: Samples were mixed with a previously prepared stock of $MgCl_2$ and chelator at a given ratio; vesicles were always mixed with premixed magnesium and chelator, so that vesicles were never exposed to unchelated magnesium. Samples were tumbled for 4 hours.
3: Vesicles were purified on Sepharose 4B size exclusion column to remove unencapsulated oligonucleotide. The mobile phase contained 75 mM vesicles with the given concentration of magnesium and chelator.
4. The fraction containing vesicles was collected. At this point, all of the oligonucleotide in the sample is encapsulated inside the vesicles.
5. Samples were incubated for a given length of time with vigorous tumbling. Samples incubated longer than 1 h were vortexed every few hours, to prevent any aggregates form forming.
6. At given time points, aliquots of vesicles were again purified on a Sepharose 4B column.
7. Leakage was calculated by quantifying the fluorescence of vesicle and small molecule fractions collected from the second column.

Figure S5

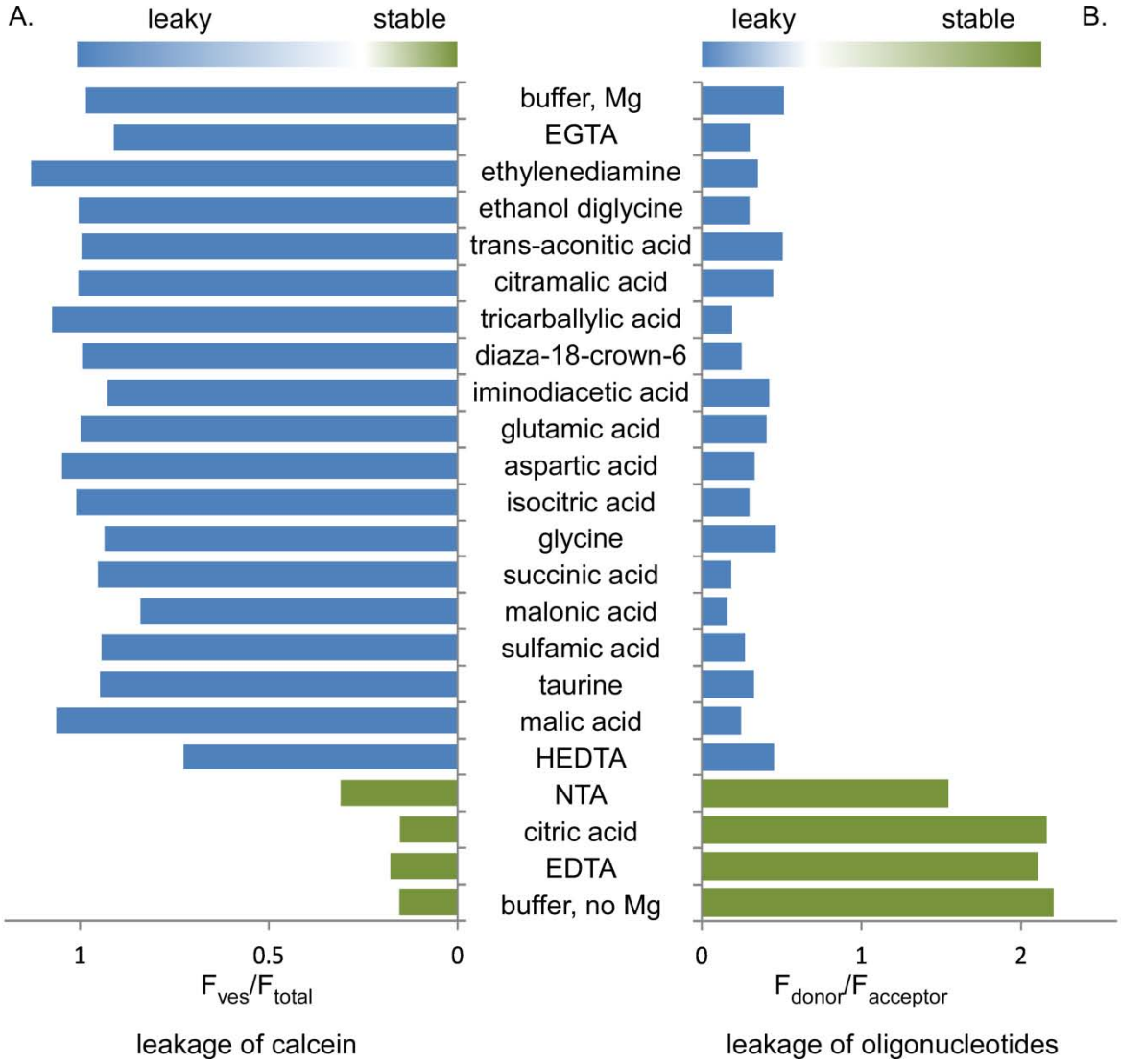

Figure S5. Summary of stability measurements of 75 mM oleic acid vesicles in presence of 50 mM magnesium and 200 mM each of different chelators.
A: Results represent measured F_{ves}/F_{total} ratio, corresponding to the dequenching of calcein and therefore the leakage of calcein across vesicle membrane. Each point is an average of fluorescence measured over 30 minutes, starting 10 h after adding magnesium and chelator to the samples.
Full time course for the experiment summarized above is on Figure S6-A.
B: Results represent measured $F_{donor}/F_{acceptor}$ ratio, corresponding to the FRET signal and therefore the leakage of oligonucleotide across vesicle membrane and loss from disrupted vesicles. Each point is an average of fluorescence measured over 30 minutes, starting 10 h after adding magnesium and chelator to the samples.
Full time course data for the experiment summarized above is on Figure S6-B.

Figure S6.

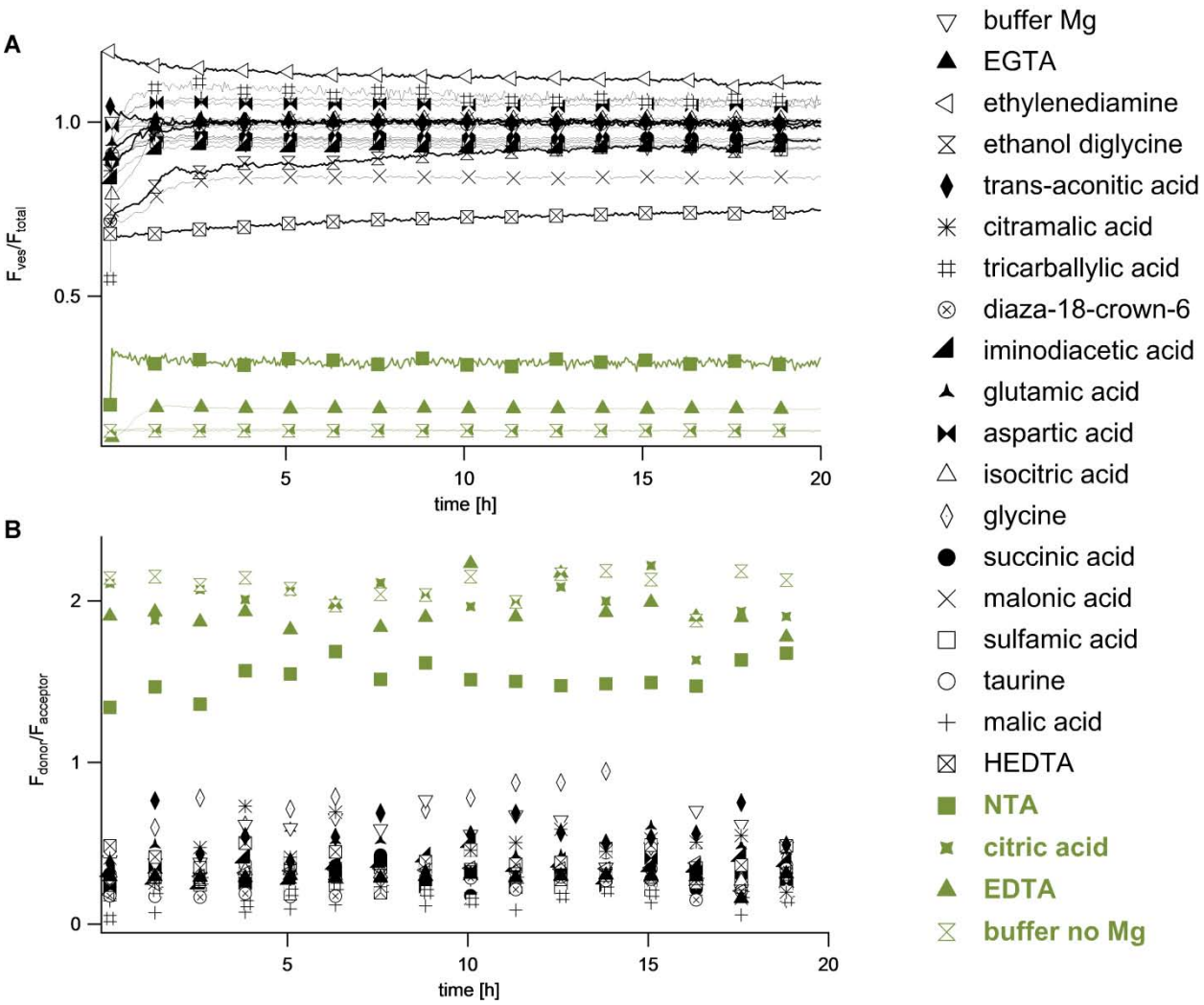

Figure S6. Stability of oleate vesicles in the presence of Mg^{2+} with different Mg^{2+} chelators.
Data obtained using kinetic leakage assays described in Figures S2 and S3 and in Materials and Methods.
Each sample: 75 mM oleic acid vesicles.
A: leakage of calcein, 200 mM each chelator, 50 mM Mg^{2+};
B: leakage of oligo d(Cy3-5′-GCGCATTGG-3′), 200 mM each chelator, 50 mM Mg^{2+}.
Green traces on each graph: most stable populations of vesicles in each experiment.

Figure S7

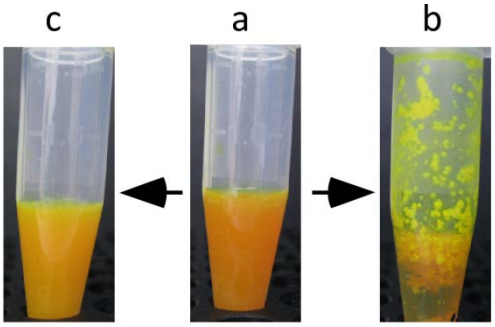

Figure S7. Citrate stabilizes fatty acid vesicles in the presence of Mg^{2+} ions.
A: 75 mM oleate vesicles form a homogeneous suspension,
B: vesicles are disrupted after the addition of 50 mM $MgCl_2$ due to the precipitation of the fatty acid,
C: vesicles remain intact after the addition of 50 mM $MgCl_2$ and 200 mM citrate.

Figure S8

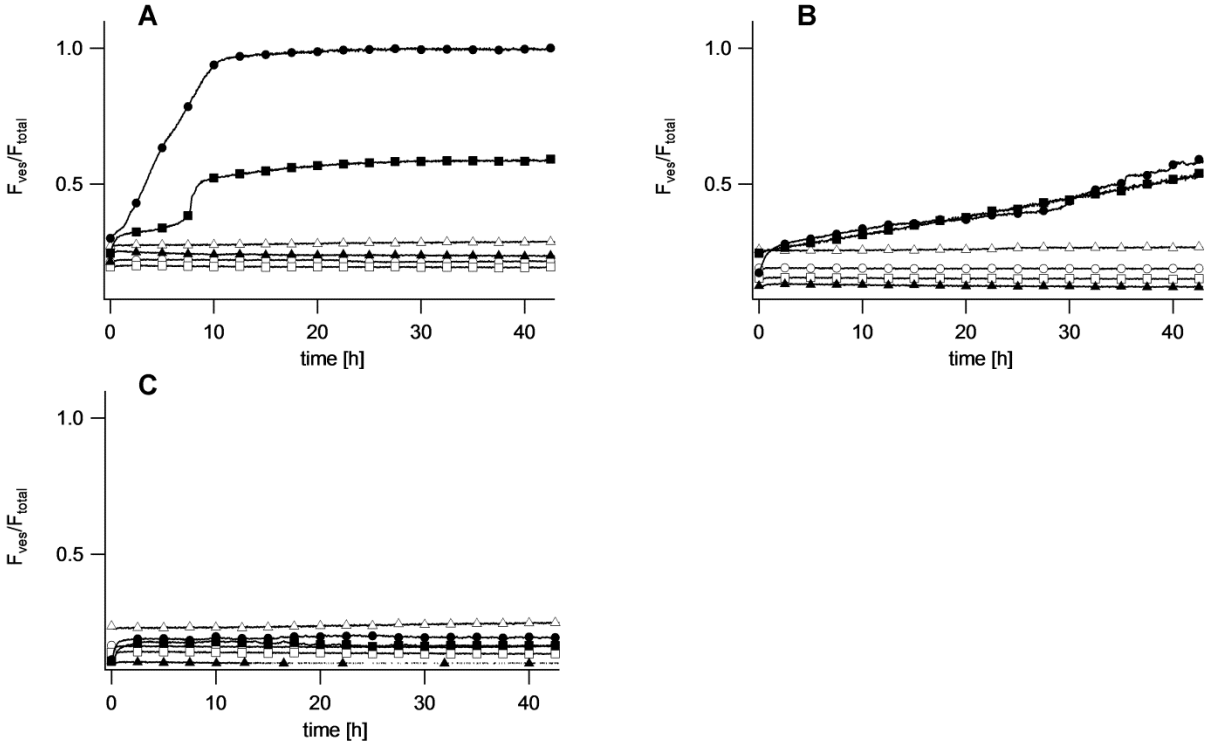

Figure S8. Leakage of calcein from 75 mM oleic acid vesicles in the presence of Mg^{2+} and citrate.
Leakage measured at different ratios of citrate to magnesium.
A: 2:1 citrate : Mg^{2+},
B: 3:1 citrate : Mg^{2+},
C: 4:1 citrate : Mg^{2+}.

▵ 10 mM Mg^{2+}, ○ 20 mM Mg^{2+}, □ 30 mM Mg^{2+}, ▲ 40 mM Mg^{2+}, ■ 50 mM Mg^{2+}, ● 60

mM Mg^{2+},
The general scheme of the assay used to obtain this data is described in Figure S1.
Data was collected every 180 seconds; markers on the graphs are placed every 50 data points (2.5 h).

Figure S9

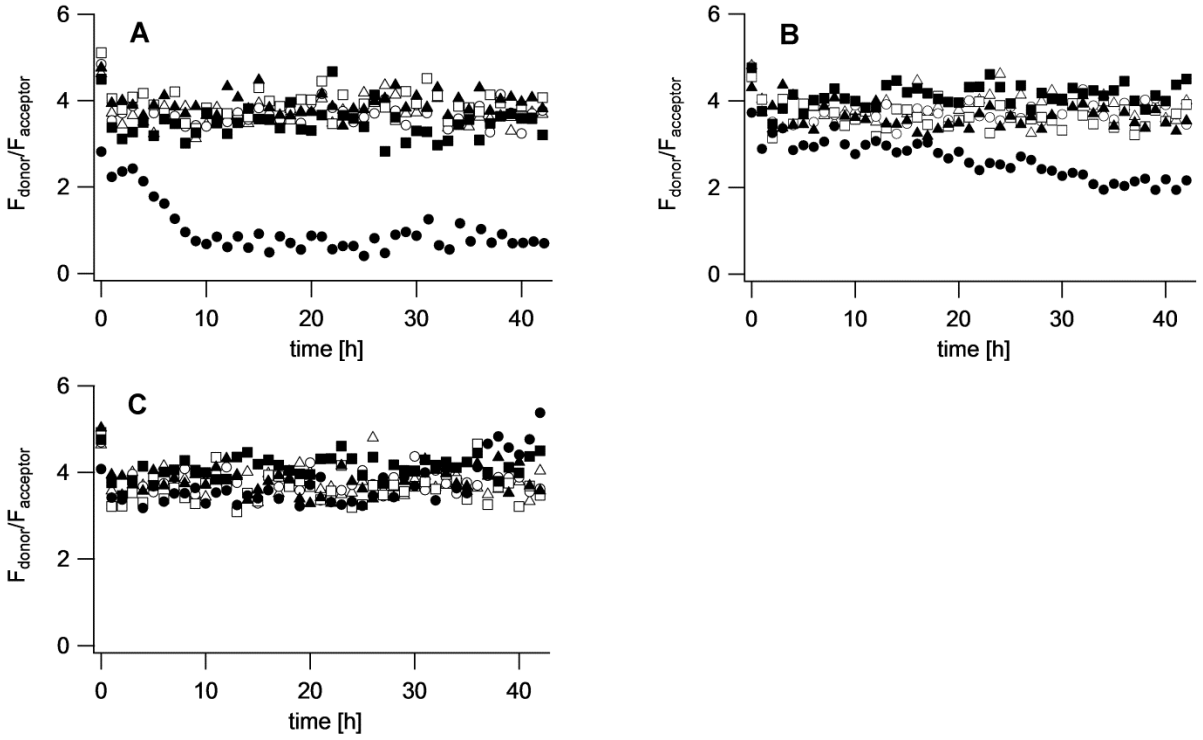

Figure S9. Leakage of oligonucleotide d(Cy3-5′-GCGCATTGG-3′) from 75 mM oleic acid vesicles in the presence of Mg^{2+} and citrate.
Leakage measured at different ratios of citrate to magnesium.
A: 2:1 citrate : Mg^{2+},
B: 3:1 citrate : Mg^{2+},
C: 4:1 citrate : Mg^{2+}.

▵ 10 mM Mg^{2+}, ○ 20 mM Mg^{2+}, □ 30 mM Mg^{2+}, ▲ 40 mM Mg^{2+}, ■ 50 mM Mg^{2+}, ● 60

mM Mg^{2+},
The general scheme of the assay used to obtain this data is described in Figure S2.
Data was collected every 180 seconds; markers on the graphs are placed every 20 data points (1 h).

Figure S10

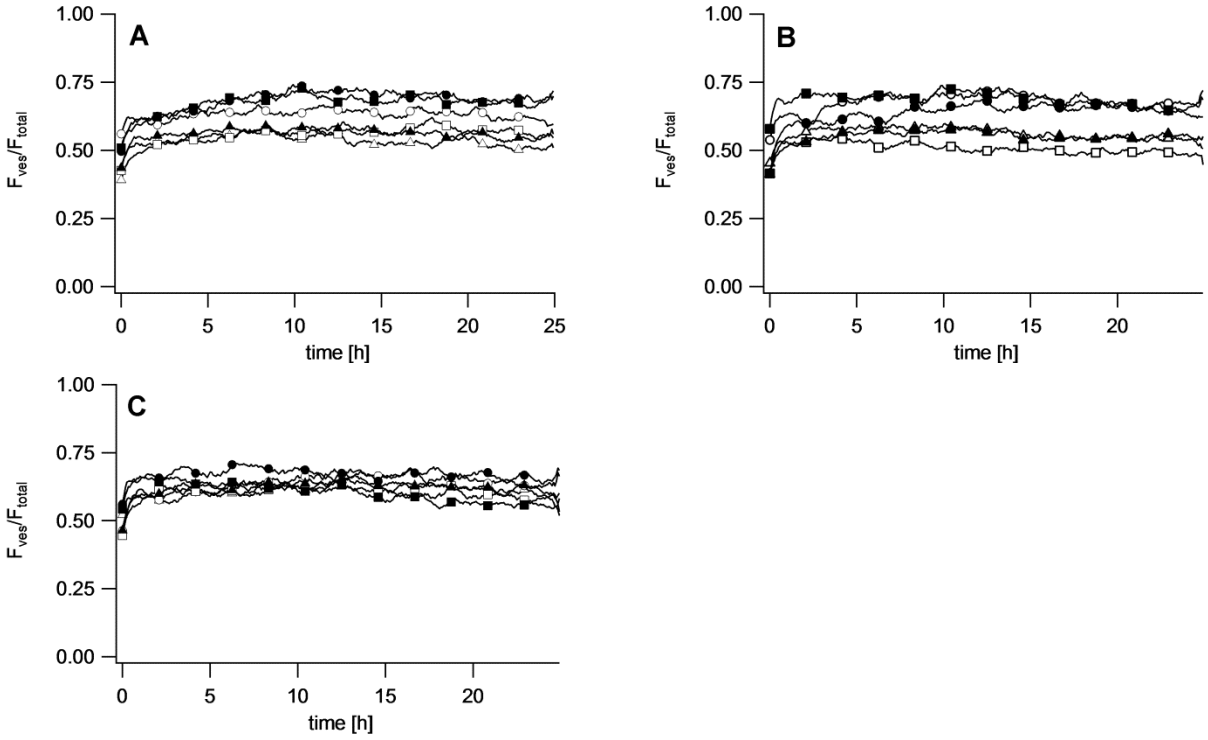

Figure S10. Leakage of calcein from 75 mM myristoleic acid : glycerol monomyristoleate 2:1 vesicles in the presence of Mg^{2+} and citrate.
Leakage measured at different ratios of citrate to magnesium.
A: 2:1 citrate : Mg^{2+},
B: 3:1 citrate : Mg^{2+},
C: 4:1 citrate : Mg^{2+}.

▵ 10 mM Mg^{2+}, ○ 20 mM Mg^{2+}, □ 30 mM Mg^{2+}, ▲ 40 mM Mg^{2+}, ■ 50 mM Mg^{2+}, ● 60 mM Mg^{2+},

The general scheme of the assay used to obtain this data is described in Figure S1.
Data was collected every 180 seconds; markers on the graphs are placed every 50 data points (2.5 h).

Figure S11

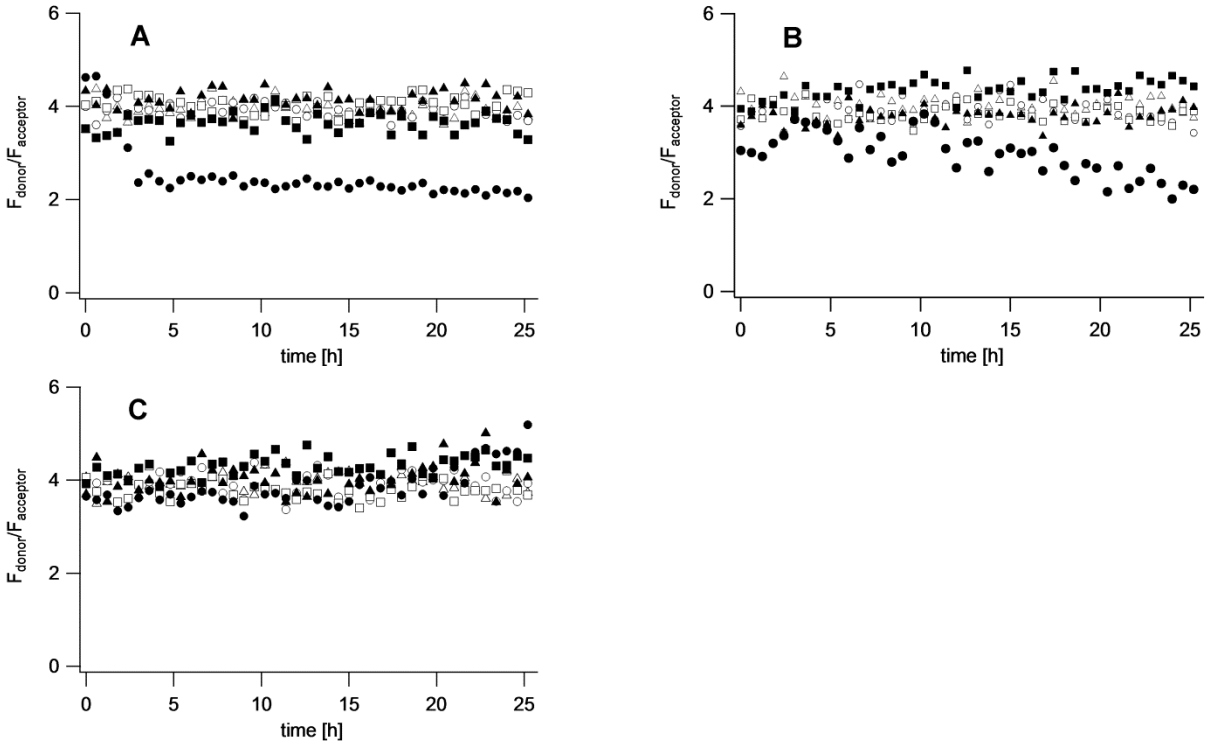

Figure S11. Leakage of oligonucleotide d(Cy3-5′-GCGCATTGG-3′) from 75 mM myristoleic acid : glycerol monomyristoleate 2:1 vesicles in the presence of Mg^{2+} and citrate.
Leakage measured at different ratios of citrate to magnesium.
A: 2:1 citrate : Mg^{2+},
B: 3:1 citrate : Mg^{2+},
C: 4:1 citrate : Mg^{2+}.

▵ 10 mM Mg^{2+}, ○ 20 mM Mg^{2+}, □ 30 mM Mg^{2+}, ▲ 40 mM Mg^{2+}, ■ 50 mM Mg^{2+}, ● 60

mM Mg^{2+},
The general scheme of the assay used to obtain this data is described in Figure S2.
Data was collected every 180 seconds; markers on the graphs are placed every 20 data points (1 h).

Figure S12

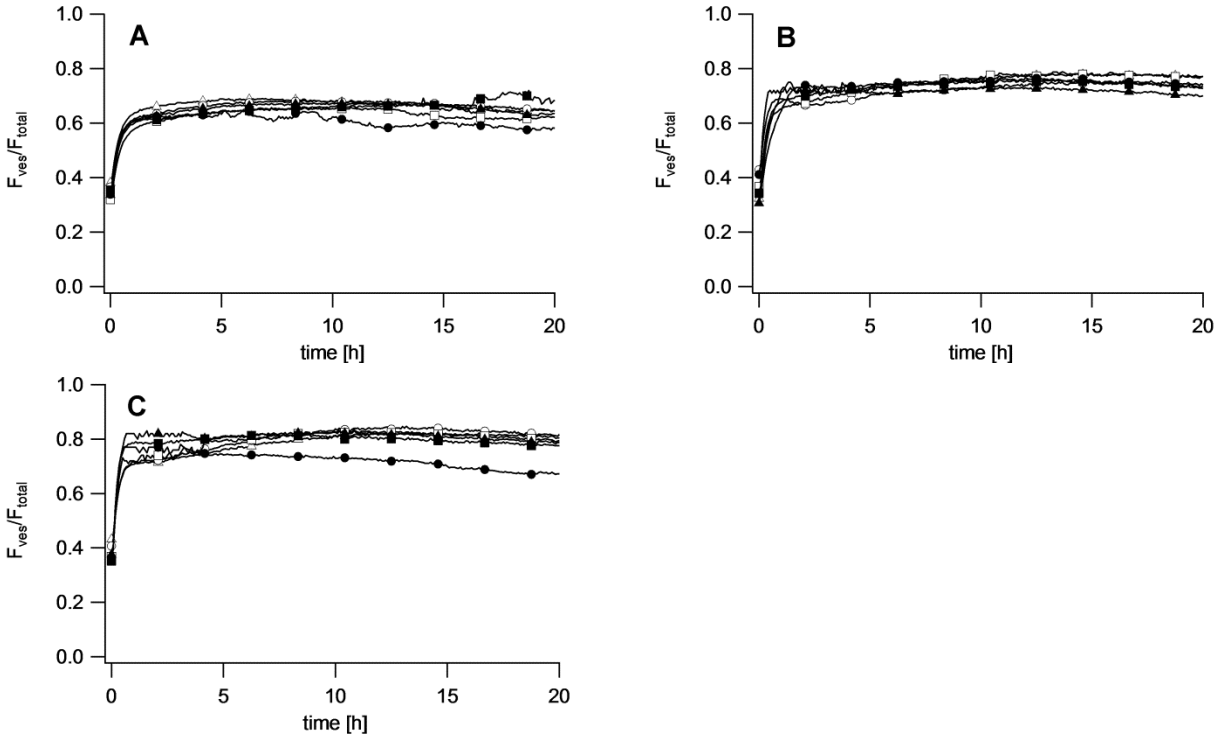

Figure S12. Leakage of calcein from 75 mM decanoic acid : decanol : glycerol monodecanoate 4:1:1 vesicles in the presence of Mg^{2+} and citrate.
Leakage measured at different ratios of citrate to magnesium.
A: 2:1 citrate : Mg^{2+},
B: 3:1 citrate : Mg^{2+},
C: 4:1 citrate : Mg^{2+}.

▵ 10 mM Mg^{2+}, ○ 20 mM Mg^{2+}, □ 30 mM Mg^{2+}, ▲ 40 mM Mg^{2+}, ■ 50 mM Mg^{2+}, ● 60

mM Mg^{2+},
The general scheme of the assay used to obtain this data is described in Figure S1.
Data was collected every 180 seconds; markers on the graphs are placed every 50 data points (2.5 h).

Figure S13

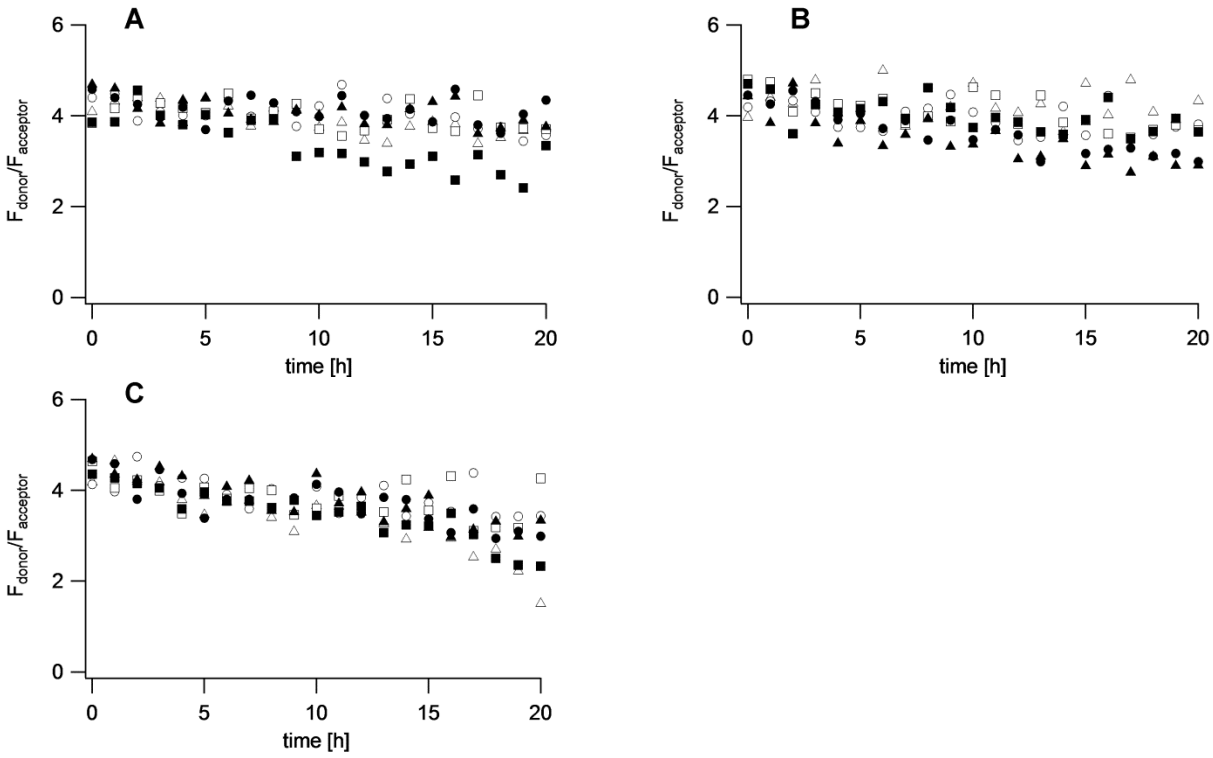

Figure S13. Leakage of oligonucleotide d(Cy3-5′-GCGCATTGG-3′) from 75 mM decanoic acid : decanol : glycerol monodecanoate 4:1:1 vesicles in the presence of Mg^{2+} and citrate.
Leakage measured at different ratios of citrate to magnesium.
A: 2:1 citrate : Mg^{2+},
B: 3:1 citrate : Mg^{2+},
C: 4:1 citrate : Mg^{2+}.

△ 10 mM Mg^{2+}, ○ 20 mM Mg^{2+}, □ 30 mM Mg^{2+}, ▲ 40 mM Mg^{2+}, ■ 50 mM Mg^{2+}, ● 60 mM Mg^{2+},
The general scheme of the assay used to obtain this data is described in Figure S2.
Data was collected every 180 seconds; markers on the graphs are placed every 20 data points (1 h).

Figure S14

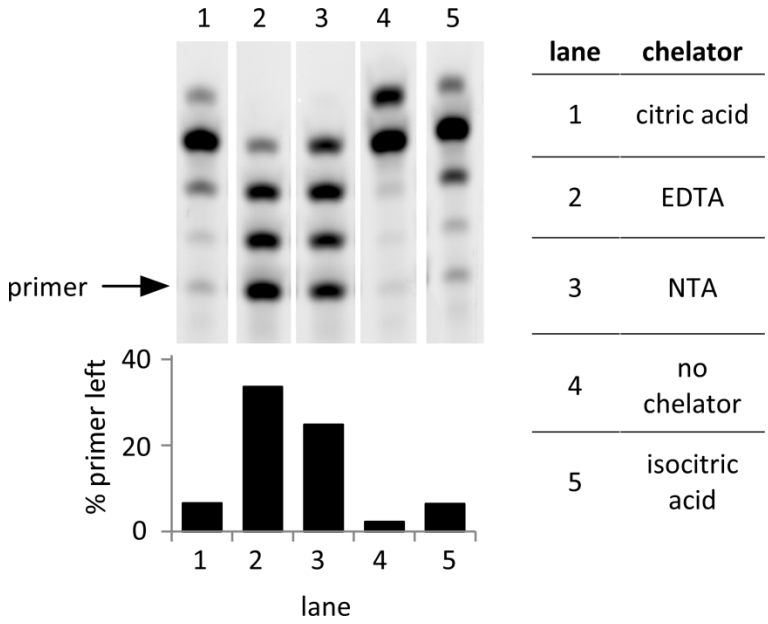

Figure S14. RNA template copying in the presence of magnesium chelators.
Each sample: 2 μM primer-G1 (5′-Cy3-GCGUAGACUGACUG-3′), 10 μM template-C4 (5′-ACCCCCAGUCAGUCUACGC-3′), 50 mM 2MeImpG, 0.25 M Tris pH 8.0, 200 mM each chelator (pH of all chelator stock solutions adjusted to 8.0), 18 h, RT.

Figure S15

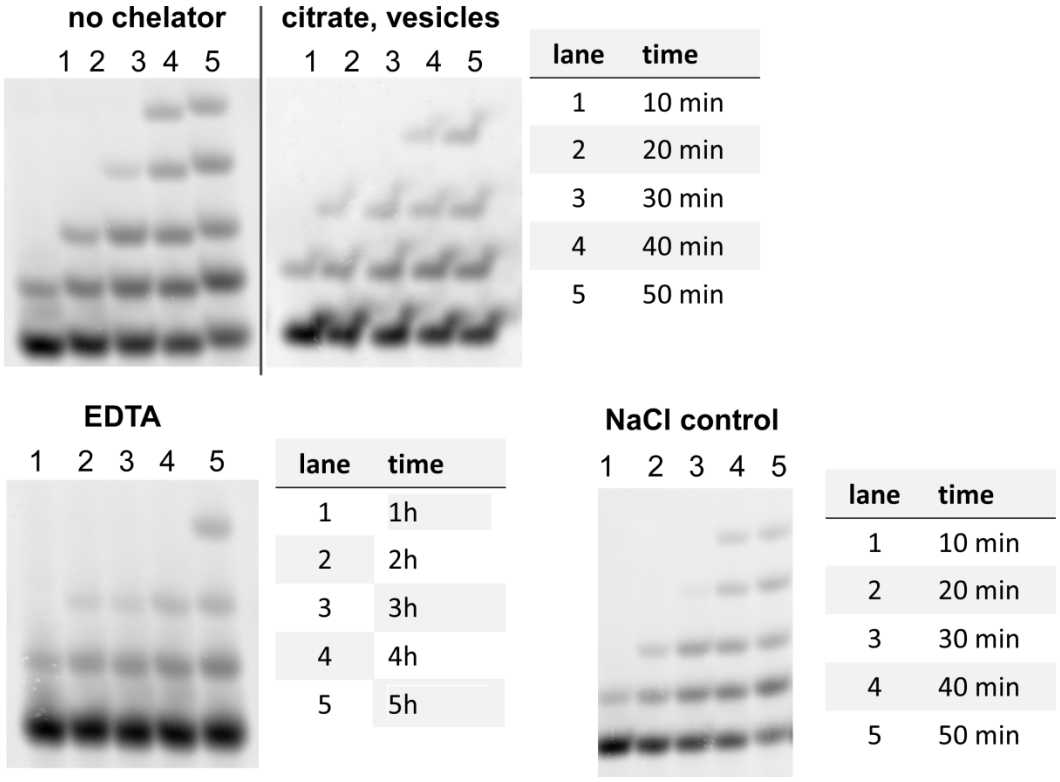

Figure S15. RNA template copying in solution in the presence/absence of chelators and in the presence of oleate vesicles
Gel analysis of time courses of RNA template copying reactions.
All samples: 2 μM primer-G1 (5′-Cy3-GCGUAGACUGACUG-3′), 10 μM template-C4 (5′-ACCCCCAGUCAGUCUACGC-3′), 50 mM MeImpG, 0.25 M Tris, 50 mM $MgCl_2$, RT. Vesicle samples: 200 mM Na^+-citrate and 100 mM oleate vesicles. EDTA samples: 200 mM EDTA.
Control NaCl: control reaction at 50 mM MeImpG, 0.25 M Tris, 50 mM $MgCl_2$ with the addition of 1.2M NaCl, to match the ionic strength of the reaction in presence of citrate. The calculated k_{obs} for this reaction (k_{obs}=1.5 h^{-1}) is in line with the k_{obs} for the unchelated reaction, reported in Figure 2 (k_{obs}=1.4 h^{-1}).
This data was used to prepare the kinetic plots on Figure 2.

Figure S16

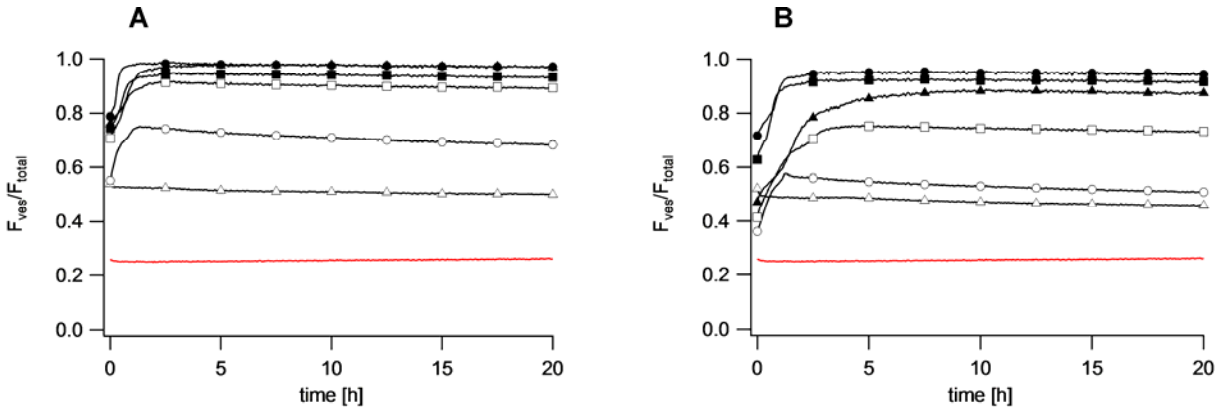

Figure S16. Leakage of calcein from 75 mM oleic acid vesicles in the presence of Mg^{2+} and isocitrate.
Leakage measured at different ratios of isocitrate to magnesium.
A: 3:1 isocitrate : Mg^{2+},
B: 4:1 isocitrate : Mg^{2+}.

∆ 10 mM Mg^{2+}, ○ 20 mM Mg^{2+}, □ 30 mM Mg^{2+}, ▲ 40 mM Mg^{2+}, ■ 50 mM Mg^{2+}, ● 60

mM Mg^{2+},
red line: no Mg^{2+} control.
The general scheme of the assay used to obtain this data is described in Figure S1.
Data was collected every 180 seconds; markers on the graphs are placed every 50 data points (2.5 h).

Figure S17

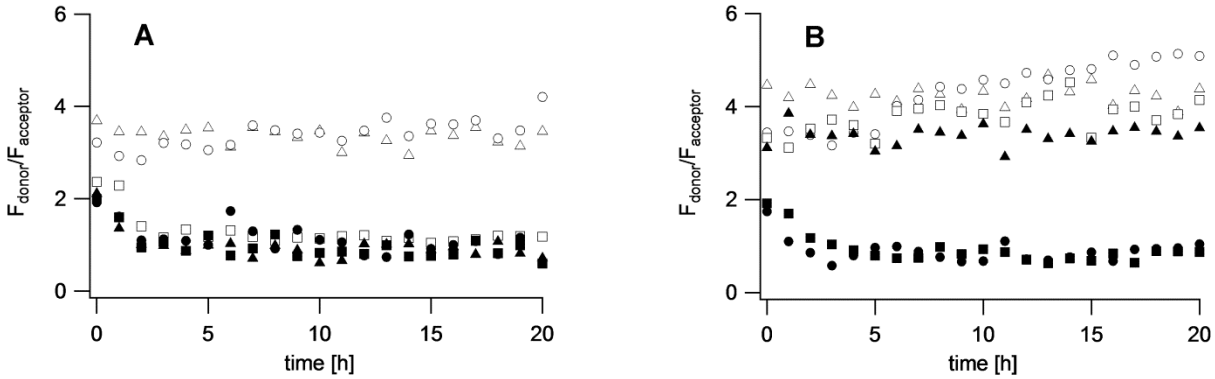

Figure S17. Leakage of oligonucleotide d(Cy3-5′-GCGCATTGG-3′) from 75 mM oleic acid vesicles in the presence of Mg^{2+} and isocitrate.
Leakage measured at different ratios of isocitrate to magnesium.
A: 3:1 isocitrate : Mg^{2+},
B: 4:1 isocitrate : Mg^{2+}.

△ 10 mM Mg^{2+}, ○ 20 mM Mg^{2+}, □ 30 mM Mg^{2+}, ▲ 40 mM Mg^{2+}, ■ 50 mM Mg^{2+}, ● 60

mM Mg^{2+},
The general scheme of the assay used to obtain this data is described in Figure S2.
Data was collected every 180 seconds; markers on the graphs are placed every 20 data points (1 h).

Figure S18

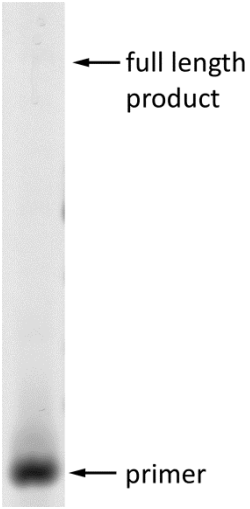

Figure S18. RNA synthesis in POPC vesicles.
2 μM primer-G1 (5′-Cy3-GCGUAGACUGACUG-3′) and 10 μM template-C4 (5′-ACCCCCAGUCAGUCUACGC-3′) were encapsulated inside 10 mM POPC (1-palmitoyl-2-oleoyl-sn-glycero-3-phosphocholine) vesicles in 0.25 M Tris. Vesicles were purified to remove unencapsulated RNA. The template copying reaction was initiated by addition of 2MeImpG and $MgCl_2$ (final concentration 50 mM 2MeImpG, 50 mM $MgCl_2$), then samples were heated up to 95 °C for 1 minute and then tumbled for 48 hours. Sample was purified and analyzed similarly do the procedure described in Materials and Methods for RNA synthesis inside fatty acid vesicles.
The primer was not extended because the monomer 2MeImpG cannot permeate phospholipid membrane.

Figure S19

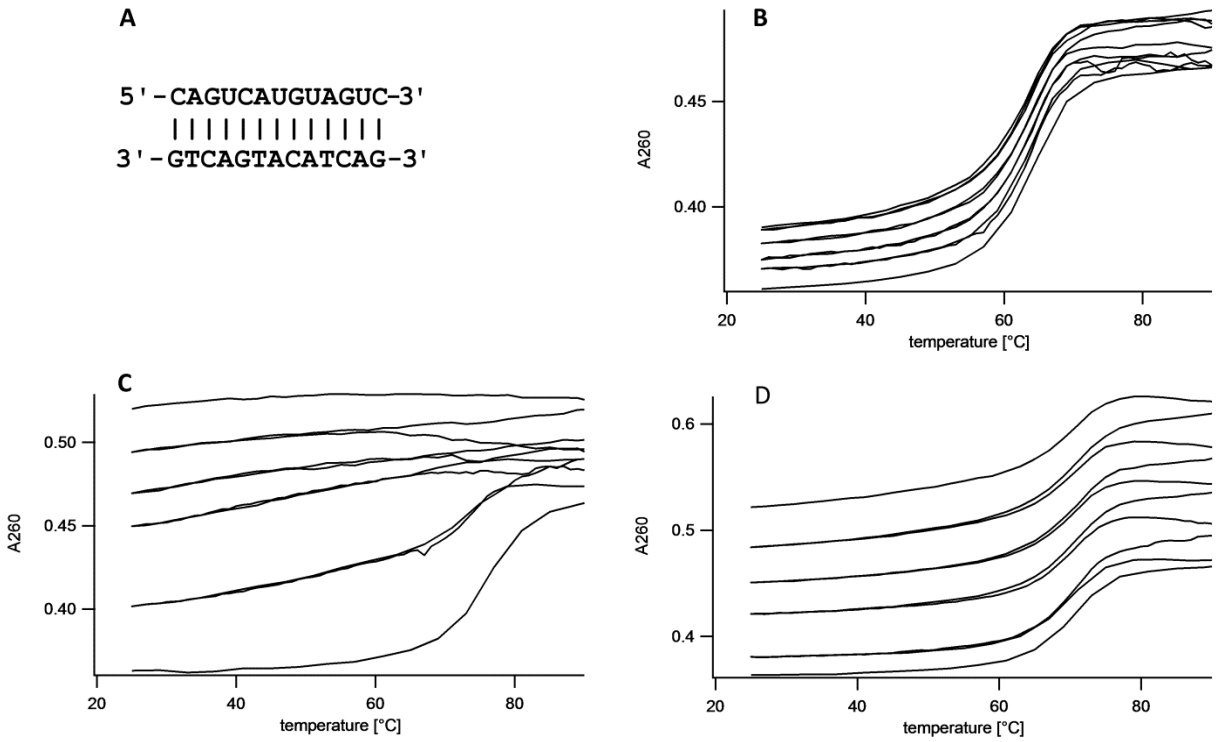

Figure S19.Thermal denaturation of a 10-mer RNA duplex in the presence of Mg^{2+} and citrate.
A: the RNA duplex formed by annealing of RNA oligos 5′-CAGUCAUGUAGUC-3′ and 3′-GUCAGUACAUCAG-5′.
B: example of RNA melting curve without magnesium and without citric acid. Curve represents repeated cycles of melting and reannealing; the absorbance increases slightly in each cycle due to degradation.
C: example of RNA melting curve with 50 mM $MgCl_2$, without citric acid. Severe RNA degradation causes a large increase in absorbance after each cycle.
D: example of RNA melting curve with 50 mM $MgCl_2$ and 200 mM citric acid. The presence of citrate decreases the absorbance increase after each cycle.
The effect of citric acid in decreasing the Tm is all the more remarkable because each equivalent of citrate comes with three equivalents of Na^+ ions, as a result of adjusting the pH of citric acid to pH 8.0 with NaOH. As a control for establishing influence of citrate on the melting temperature of the RNA duplex, we used samples with 3 equivalents of NaCl for each citric acid concentration, to reproduce the monovalent cations concentration in the citrate samples.

Figure S20

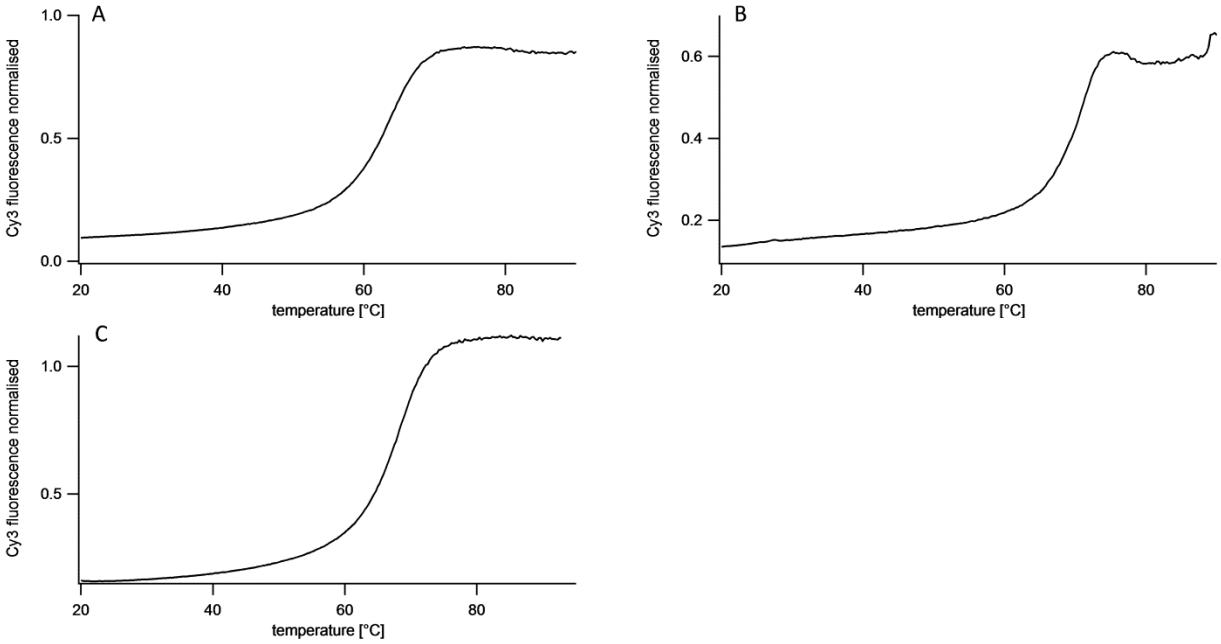

Figure S20. Thermal denaturation of 10-mer RNA duplex in the presence of vesicles, Mg^{2+} and citrate.
RNA oligonucleotides: 5′-GACUACAUGACUG-Cy5 and 5′-Cy3-CAGUCAUGUAGUC-3′.
A: example of RNA melting curve with 100 mM oleic acid vesicles, without Mg^{2+} and without citrate;
B: example of RNA melting curve with 100mM oleic acid vesicles, with 50 mM $MgCl_2$ and 200 mM citrate;
C: example of RNA melting curve without vesicles, with 50 mM $MgCl_2$ and 200 mM citrate.
Results are summarized in Table S2.
For detailed description of the procedure see Materials and Methods.

Figure S21

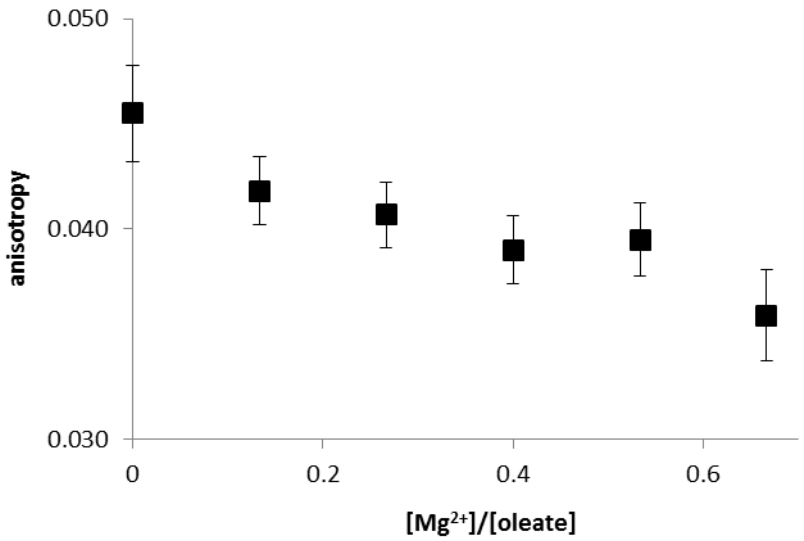

Figure S21. Anisotropy of oleate protocell vesicle membrane in the presence of Mg^{2+} and citrate (4x citrate relative to Mg^{2+}).
Error bars indicate SEM (N=10).
Total lipid concentration in each sample 75 mM, including 8 mM of oleate vesicles with 0.25 mol% of DPH (1,6-Diphenyl-1,3,5-hexatriene). Each sample 0.25 M Tris pH 8.0.

Table S1.

ratio citrate/Mg^{2+}	10mM Mg^{2+}	NaCl control*	50mM Mg^{2+}	NaCl control*
-	69°C	-	75°C	-
2	65°C	71°C	70°C	74°C
3	65°C	70°C	70°C	75°C
4	66°C	71°C	71°C	75°C

*NaCl was used at 3x the concentration of citrate (in addition to 0.1M NaCl in each sample), to match the salinity of the respective citric acid sample.

Table S1. Influence of citrate on the melting temperature (T_m) of a 10-mer RNA duplex Each sample contained 15 µM of RNA oligonucleotides 5′-CAGUCAUGUAGUC and 5′-GACUACAUGACUG, 1 mM EDTA, 0.1 M NaCl and 0.25 M Tris-Cl pH 8.0.

Table S2.

```
Primer-G4 5′-Cy3-GCG UAG ACU GAC UG -3′
                  ||| ||| ||| ||| ||
Template-C4   3′-CGC AUC UGA CUG AC CCCC A -5′
```

calculated T_m of duplex [1]

primer – template	83.5 °C
fully extended primer – template	97.0 °C

```
Primer-G7 5′-Cy3-GCG UAG ACU GAC UGG -3′
                  ||| ||| ||| ||| |||
Template-C7   3′-CGC AUC UGA CUG ACC CCCCCCC AA -5′
```

calculated T_m of duplex [1]

primer – template	88.0 °C
fully extended primer – template	107.0 °C

calculated T_m of most stable hairpin [2]

primer	45.6 °C
template	34.2 °C
fully extended primer	45.6 °C

Primer-GC 5′-Cy3-GCG UAG ACU GAC UGG -3′

||| ||| ||| ||| |||

Template-GC 3′-CGC AUC UGA CUG ACC GCCG A -5′

calculated T_m of duplex [1]

primer – template	87.8 °C
fully extended primer – template	99.3 °C

Table S3. Stability of primer-template complexes used in RNA template copying reactions.
Sources of data:
1: Hy-Ther version 1.0, Nicolas Peyret and John SantaLucia, Jr., Wayne State University. Tm calculated for 0.25M monovalent cations and 50mM Mg^{2+} at 2 µM of each strand.
2: Oligo Analyzer version 3.1 by Integrated DNA Technologies

Table S3

no Mg^{2+}, no citrate			
vesicles		NaCl control	
0 mM	63°C	-	-
75 mM	63°C	75 mM	64°C

50 mM Mg^{2+}, 200 mM citrate			
vesicles		NaCl control	
0 mM	68°C	-	-
75 mM	69°C	75 mM	68°C

Table S2. T_m of 10-mer RNA duplex in presence of vesicles.
RNA oligonucleotides: 5′-GACUACAUGACUG-Cy5 and 5′-Cy3-CAGUCAUGUAGUC-3′. Each sample 0.25 M Tris pH 8.0. Examples of melt traces are shown on Figure S18.

Liposome reactor dialyzer

General description

The liposome reactor dialyzer allows dialysis of small volume samples with a relatively large dialysis membrane surface area. The dialyzer is light and portable; it can be placed on a shaker or on vertical rotator. This is important in the case of liposome reactions, where samples need to be tumbled during the extended reaction time. The dialyzer can be easily heated up or cooled down, allowing for rapid cycling of the reaction temperature. The dialyzer consists of two chambers; the maximum volume of sample that can be placed in each chamber is 250 µL. The effective dialysis area is 1.56 cm^2. The dialyzer is built by modifying commercially available Thermo Scientific Slide-A-Lyzer Dialysis Cassettes.

General scheme of the liposome reactor dialyzer

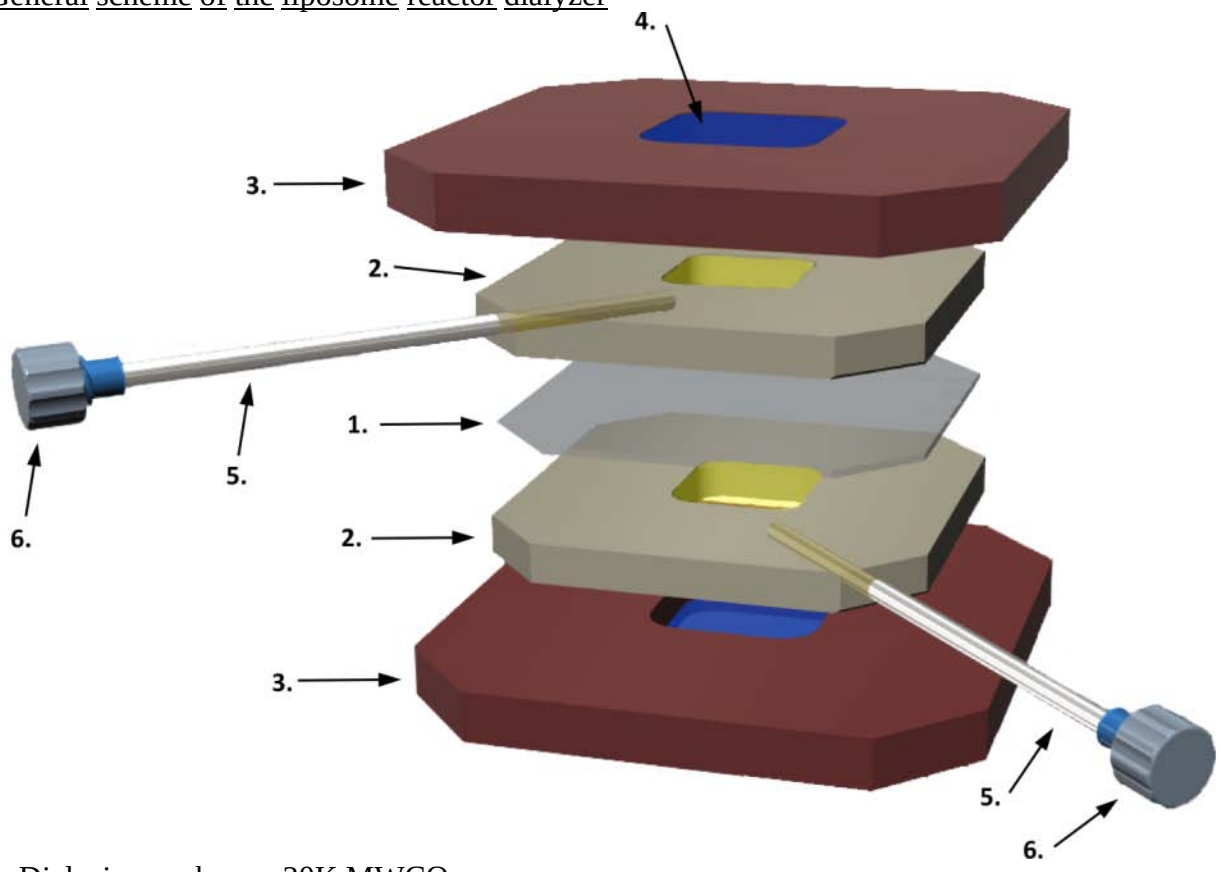

1. Dialysis membrane, 20K MWCO
2. Silicone gaskets
3. Plastic cassette, top and bottom
4. The window on either side of the plastic cassette, sealed with the PCR film
5. Needles for loading sample and wash buffers
6. Needle luer caps
Sample chambers are yellow colored.

Example of use of vesicle dialyzer: non-enzymatic template-directed RNA synthesis

RNA primer and template were encapsulated inside protocell fatty acid vesicles. Protocells with RNA are injected into the sample chamber of the dialyzer. The dialysis exchange chamber is filled with solution containing empty fatty acid vesicles and buffer of the same composition as the sample chamber, plus the imidazole activated RNA monomer. The monomer is dialyzed into the sample chamber, diffuses inside the protocells and the RNA primer is extended. The products of the spontaneous hydrolysis of the imidazole activated monomer in the sample chamber are dialyzed into the exchange chamber and removed with each exchange of the buffer.

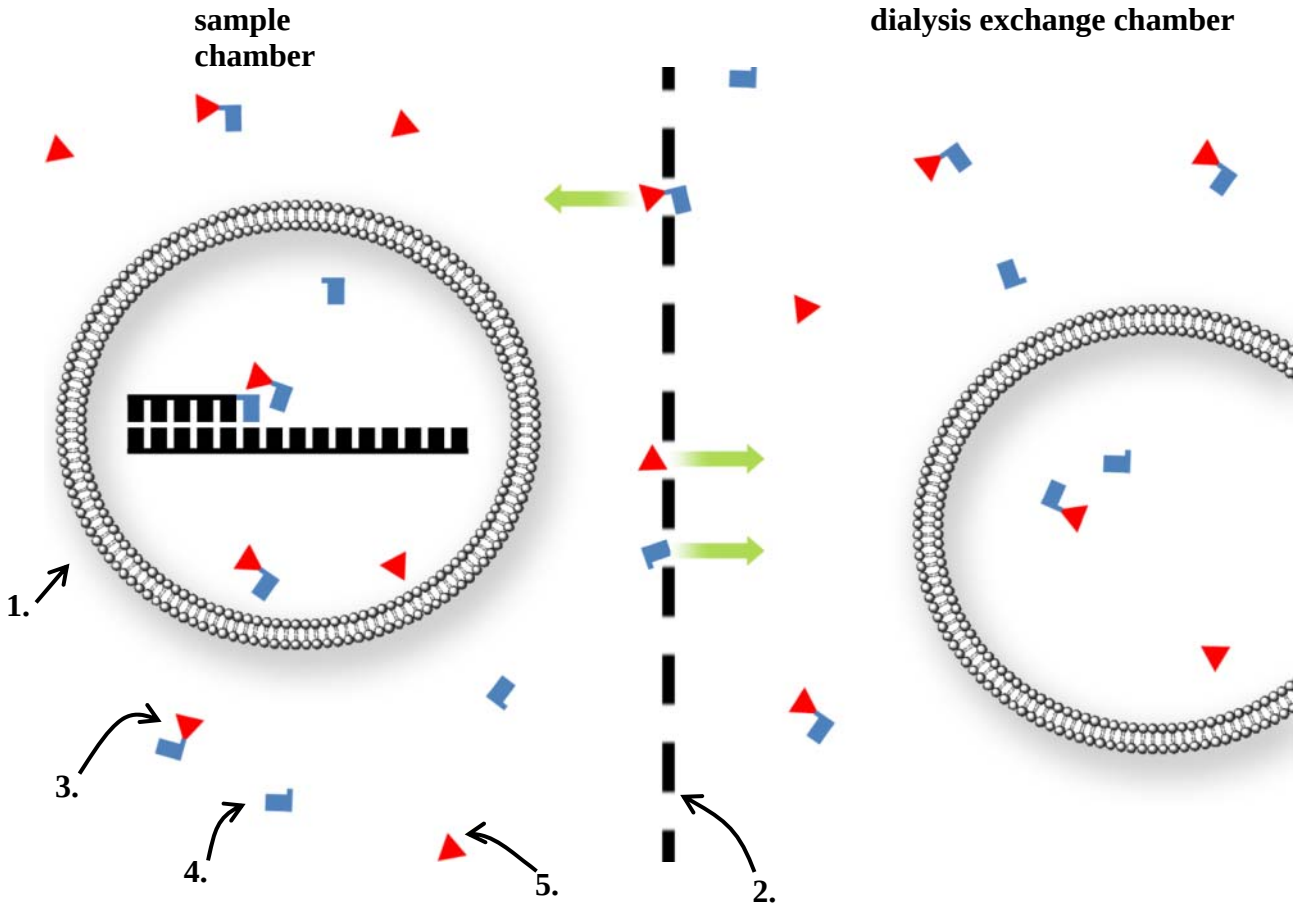

1. Protocell vesicles with encapsulated template and primer RNA in the sample chamber. The new strand of RNA is synthesized inside the protocell, using as a substrate activated RNA monomer delivered from the dialysis exchange chamber.
2. Dialysis membrane.
3. Substrate for RNA synthesis: imidazole activated RNA monomer.
4. Hydrolyzed RNA monomer and **5.** hydrolyzed activation group, the imidazole. The products of hydrolysis of imidazole activated RNA monomer are removed from the site of the RNA synthesis reaction through dialysis membrane to the exchange chamber.

Witch each exchange of the buffer in the dialysis exchange chamber, a fresh portion of activated RNA monomer is delivered and products of hydrolysis of the activated monomer are removed.

RNA synthesis inside protocell vesicles with dialysis proceeds with much higher yields than comparable reaction in solution or in vesicles without dialysis.
The imidazole activated RNA monomers hydrolyze to the monophosphate and imidazole in aqueous solutions with half-life of several hours. The vesicle dialyzer allows for multiple delivery of fresh activated monomer, and removal of products of monomer hydrolysis that would inhibit the RNA synthesis reaction.
The relatively large dialysis surface, and small volumes of both sample and dialysis exchange buffer, minimize the loss of monomers and maximize the dialysis efficiency.

References and Notes

1. W. Gilbert, Origin of life: The RNA world. *Nature* **319**, 618 (1986). doi:10.1038/319618a0

2. G. F. Joyce, RNA evolution and the origins of life. *Nature* **338**, 217–224 (1989). doi:10.1038/338217a0 Medline

3. J. M. Gebicki, M. Hicks, Ufasomes are stable particles surrounded by unsaturated fatty acid membranes. *Nature* **243**, 232–234 (1973). doi:10.1038/243232a0 Medline

4. D. W. Deamer, J. P. Dworkin, Chemistry and physics of primitive membranes. *Top. Curr. Chem.* **259**, 1–27 (2005). doi:10.1007/b136806

5. J. W. Szostak, The eightfold path to non-enzymatic RNA replication. *J. Sys. Chem.* **3**:2 (2012).

6. J. C. Bowman, T. K. Lenz, N. V. Hud, L. D. Williams, Cations in charge: Magnesium ions in RNA folding and catalysis. *Curr. Opin. Struct. Biol.* **22**, 262–272 (2012). doi:10.1016/j.sbi.2012.04.006 Medline

7. S. S. Mansy, J. W. Szostak, Thermostability of model protocell membranes. *Proc. Natl. Acad. Sci. U.S.A.* **105**, 13351–13355 (2008). doi:10.1073/pnas.0805086105 Medline

8. C. Deck, M. Jauker, C. Richert, Efficient enzyme-free copying of all four nucleobases templated by immobilized RNA. *Nat. Chem.* **3**, 603–608 (2011). doi:10.1038/nchem.1086 Medline

9. A. K. Covington, E. Y. Danish, Measurement of magnesium stability constants of biologically relevant ligands by simultaneous use of pH and ion-selective electrodes. *J. Solution Chem.* **38**, 1449–1462 (2009). doi:10.1007/s10953-009-9459-3

10. M. Walser, Ion association V. Dissociation constants for complexes of citrate with sodium, potassiun, calcium, and magnesium ions. *J. Phys. Chem.* **65**, 159–161 (1961). doi:10.1021/j100819a045

11. C. K. Johnson, X-ray crystal analysis of the substrates of aconitase. V. Magnesium citrate decahydrate $[Mg(H_2O)_6][MgC_6H_5O_7(H_2O)]_2 . 2H_2O$. *Acta Crystallogr.* **18**, 1004–1018 (1965). doi:10.1107/S0365110X6500244X Medline

12. C. Butch, E. D. Cope, P. Pollet, L. Gelbaum, R. Krishnamurthy, C. L. Liotta, Production of tartrates by cyanide-mediated dimerization of glyoxylate: A potential abiotic pathway to the citric acid cycle. *J. Am. Chem. Soc.* **135**, 13440–13445 (2013). doi:10.1021/ja405103r Medline

13. G. F. Joyce, T. Inoue, L. E. Orgel, Non-enzymatic template-directed synthesis on RNA random copolymers: Poly(C, U) templates. *J. Mol. Biol.* **176**, 279–306 (1984). doi:10.1016/0022-2836(84)90425-X Medline

14. T. F. Zhu, K. Adamala, N. Zhang, J. W. Szostak, Photochemically driven redox chemistry induces protocell membrane pearling and division. *Proc. Natl. Acad. Sci. U.S.A.* **109**, 9828–9832 (2012). doi:10.1073/pnas.1203212109 Medline

15. T. F. Zhu, J. W. Szostak, Coupled growth and division of model protocell membranes. *J. Am. Chem. Soc.* **131**, 5705–5713 (2009). doi:10.1021/ja900919c Medline